Fall 2015

Systemic Insulin Sensitivity and Skeletal Muscle Akt Signaling in Rats Artificially Selected for Low and High Aerobic Capacity

Kyle Levi Fulghum

SYSTEMIC INSULIN SENSITIVITY AND SKELETAL MUSCLE AKT SIGNALING IN RATS ARTIFICIALLY SELECTED FOR LOW AND HIGH AEROBIC CAPACITY

A Masters Thesis

Presented to

The Graduate College of

Missouri State University

In Partial Fulfillment

Of the Requirements for the Degree

Master of Science, Cell and Molecular Biology

By

Kyle Fulghum

December 2015

SYSTEMIC INSULIN SENSITIVITY AND SKELETAL MUSCLE AKT SIGNALING IN RATS ARTIFICIALLY SELECTED FOR LOW AND HIGH AEROBIC CAPACITY

Biomedical Sciences

Missouri State University, December 2015

Master of Science

Kyle Fulghum

ABSTRACT

The mechanism(s) linking physical inactivity, obesity, and type-II diabetes are unclear. I hypothesized low intrinsic aerobic capacity is associated with reduced systemic insulin sensitivity via skeletal muscle insulin signaling. After 34 generations of selective breeding, high aerobic capacity (HCR) rats exhibited an 8-fold increase in running distance vs low aerobic capacity (LCR) rats (*n*=14 per group). LCR rats had higher rates of weight gain vs HCR ($p<0.05$) though food consumption was constant ($p=0.86$) over a 12-week study. Rats were divided into 4 groups: 1) LCR-Sham Surgery, 2) LCR-Catheterization, 3) HCR-Sham Surgery or 4) HCR-Catheterization (*n*=7 per group). Euglycemic-hyperinsulinemic clamps on catheterized rats tested insulin sensitivity while sham LCR and HCR were used for basal tissue analysis. Plasma insulin levels did not differ during the clamps, but LCR required lower glucose infusion rates than HCR ($p<0.05$). Upon insulin stimulation, both absolute and normalized phospho-Akt(Ser^{473}) of soleus muscle were significantly increased in HCR above basal group ($p<0.05$), but not in LCR. No difference was observed between insulin-stimulated phospho-Akt(Ser^{473}) of HCR and LCR groups . These data support that LCR is linked to a reduction in insulin sensitivity *in vivo* without impairments of insulin-stimulated skeletal muscle phospho-Akt(Ser^{473}) vs HCR rats.

KEYWORDS: aerobic capacity, insulin signaling, Akt, metabolism, skeletal muscle, rat

This abstract is approved as to form and content

_____

R. Tyler Morris, PhD
Chairperson, Advisory Committee
Missouri State University

SYSTEMIC INSULIN SENSITIVITY AND SKELETAL MUSCLE AKT SIGNALING IN RATS ARTIFICIALLY SELECTED FOR LOW AND HIGH AEROBIC CAPACITY

By

Kyle Fulghum

A Masters Thesis
Submitted to the Graduate College
Of Missouri State University
In Partial Fulfillment of the Requirements
For the Degree of Master of Science, Cell and Molecular Biology

December 2015

Approved:

_____
R. Tyler Morris, PhD

_____
Benjamin Timson, PhD

_____
Scott Zimmerman, PhD

_____
Julie Masterson, PhD: Dean, Graduate College

ACKNOWLEDGEMENTS

I dedicate this thesis to everyone who helped me get where I am today.

To my committee: thank you for your insight and patience as I worked to grasp concepts and apply them to my research. In addition, I appreciate your helpfulness and support throughout this entire process.

To my fellow graduate students: thank you for suffering with me through late nights and never-ending laboratory procedures. I am not sure if I would have retained any sanity if it were not for your comedic relief, shared struggles, and continual encouragement.

To my family: thank you for years and years of support. You have never doubted me, and I always appreciate your efforts to lift my spirits.

To Dr. Morris: thank you for putting up with me during this project. We shared many early mornings and long weeks in the lab. I appreciate your constant encouragement, insight, and support – even when I didn't seem to understand things. You are great mentor and role model.

Special thanks to Katelyn Moore, Margaret Thornton, Scott Zimmerman, Benjamin Timson, Lauren Koch, Steve Britton, and Tyler Morris for direct assistance in the completion of this thesis.

TABLE OF CONTENTS

LIST OF FIGURES

INTRODUCTION

Diabetes, Obesity, and Physical Inactivity

The mechanism linking diabetes, obesity, and physical inactivity is unknown; however, an integrated relationship appears to exist (Figure 1). Obesity increases the risk for diabetes, and insulin resistance has been shown to develop in those who are obese (Dwyer-Lindgren et al. 2013; Shulman 2000). Physical inactivity has been linked to an increased risk of obesity as well. Sedentary behaviors demonstrate up to a 61% increase in the risk for developing obesity (Tremblay and Willms 2003). Physical inactivity has been demonstrated to reduce insulin sensitivity. After two weeks of reduced activity, the body becomes less insulin-sensitive (Krogh-Madsen et al. 2010).

The centers for disease control and prevention (CDC) state that only 48% of adults met physical activity guidelines in 2008 (Centers for Disease Control 2014). This proportion is important, as the CDC links physical inactivity to an increase in risk factors for complex diseases (Centers for Disease Control 2011).

There is a link between physical inactivity as it relates to the complex disease phenotype of diabetes (Figure 1) Physical inactivity is associated with increased insulin resistance, which is characteristic of type-II diabetes mellitus (TIIDM). Regions with lower proportions of physical inactivity and lower proportions of obesity tend to have a lower incidence of diabetes (Centers for Disease Control 2009). Taken together, there appears to be an association between physical inactivity, obesity, and the occurrence of diabetes.

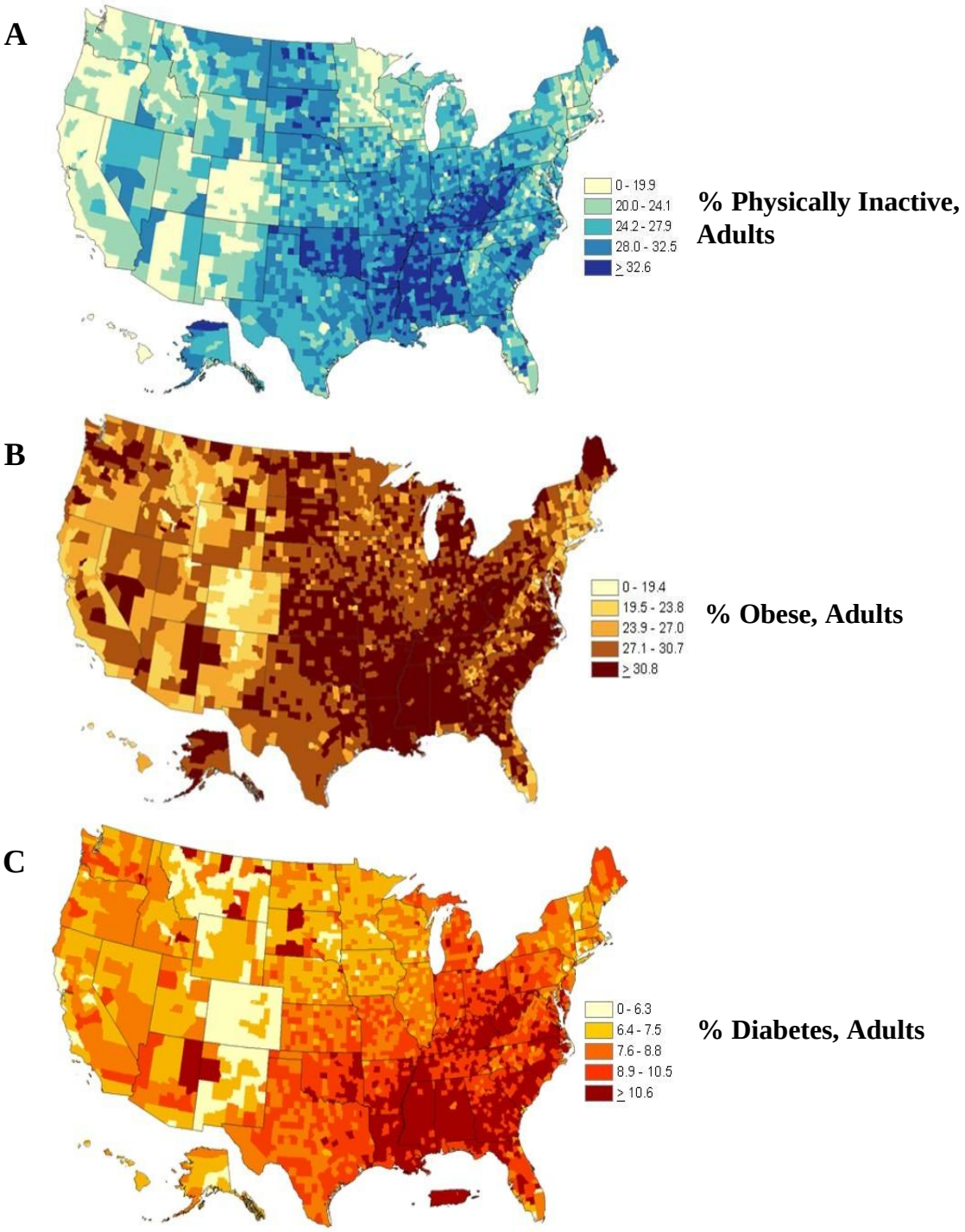

Figure 1: Geographical proportion of physical inactivity **(A)**, obesity **(B)**, and diabetes **(C)** within the Unites States in 2009. The darker shaded regions represent a higher percentage of the regional population who fit the description. Southern and Southeastern regions appear to have the darkest shading, indicating the highest incidences of all three phenomena. This suggests a potential link between these observations (Centers for Disease Control 2009).

Insulin Resistance as a Common Mechanism?

Insulin resistance is a precursor to diabetes and has been shown to develop in obesity (Shulman 2000). Physical inactivity has also been linked to a reduction in peripheral insulin sensitivity, which leads to insulin resistance (Figure 2). Insulin resistance results in a reduction in glucose uptake into cells and is associated with TIIDM (Karp 2010; Campbell and Reece 2005). A reduction in insulin sensitivity is hallmark of insulin resistance. This causes a reduction in insulin signaling, altering the activation of several pathways within the cell (Karp 2010). Normal insulin signaling results in adequate glucose uptake for appropriate energy metabolism. These observations support an association of insulin resistance with diabetes, physical inactivity, and obesity, which may suggest insulin resistance is a common mechanism linking these phenomena.

Insulin resistance is pronounced in skeletal muscle tissue (Wasserman and Ayala 2005). Skeletal muscle tissue comprises much of body mass and is a major consumer of blood glucose. This is because skeletal muscle not only demands energy production for cellular processes, but also for force generation in mobility (Sasson et al. 1987). To fully understand the impact of insulin resistance, one must be familiar with the process of insulin-stimulated glucose uptake (Figure 3).

Insulin Signaling and the Effects of Insulin Resistance

Insulin is a peptide hormone generally associated with the regulation of blood glucose concentration. It is synthesized in β-cells within islets of Langerhans in the pancreas. After a meal, carbohydrates are degraded into simple sugars and absorbed into the bloodstream, therefore raising blood glucose levels. Due to the high glucose affinity

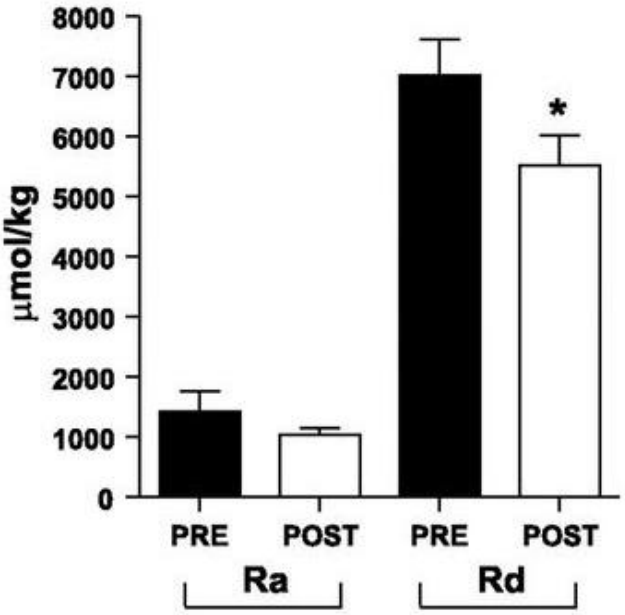

Figure 2: Two weeks of reduced ambulatory activity reduces peripheral insulin signaling (Krogh-Madsen et al. 2010). In the x-axis of this figure, Ra refers to hepatic glucose production and Rd refers to glucose disappearance. The black bars indicate normal ambulatory activity whereas the white bars indicate post-intervention of two weeks reduction in ambulatory activity. In this figure, the y-axis refers to µmol/kg of glucose. These data demonstrate no difference in hepatic glucose production after two weeks of reduced ambulatory activity, $p>0.05$. However, there is a significant decrease in glucose disappearance rate after the reduction in ambulatory activity, $*p=0.01$. Figure and data taken from (Krogh-Madsen et al. 2010).

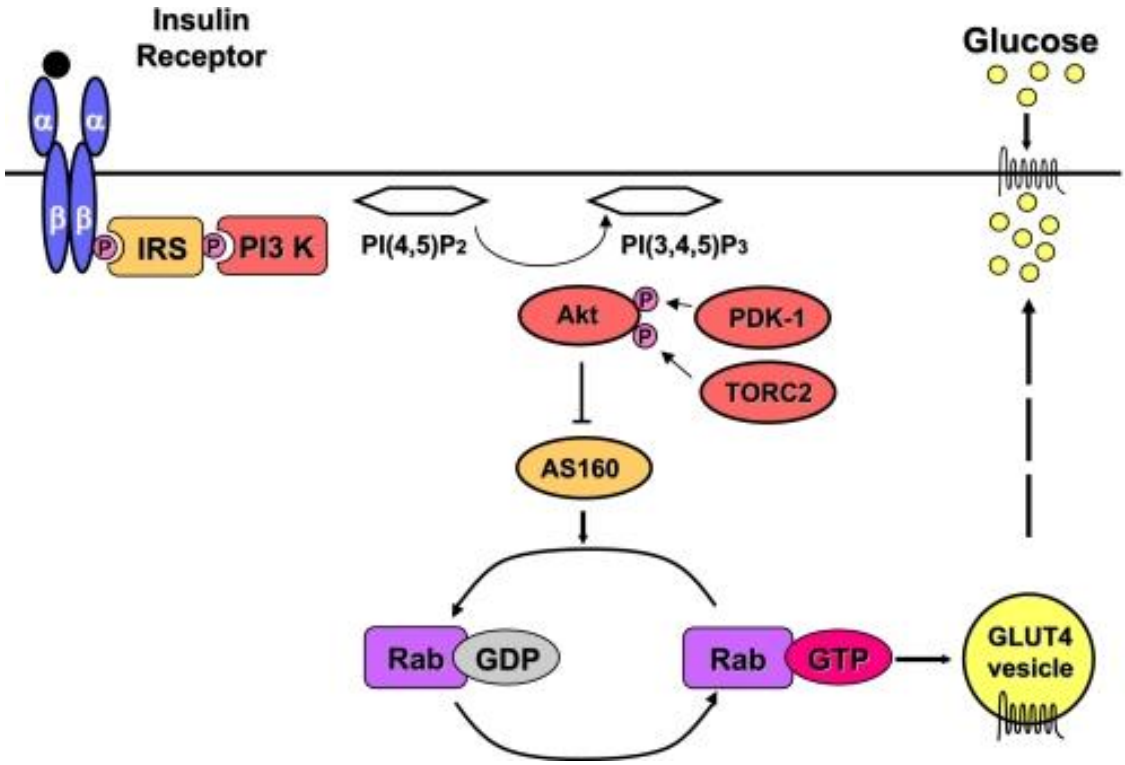

Figure 3: Schematic illustration of insulin-stimulated GLUT4 translocation (Dash et al. 2009). Insulin binding leads to recruitment and activation of the insulin receptor substrate (IRS) and subsequent recruitment of phosphatidylinositol 3 kinase (PI3K). This recruitment catalyzes conversion of PIP2 to PIP3, which causes phosphorylation of Akt via PDK1and TORC2. Akt phosphorylates AS160 and suppresses GAP activity, which then leads to an increase in GTP-bound Rab proteins that facilitate GLUT4 vesicle translocation to the membrane. Figure taken from (Dash et al. 2009).

of GLUT2 within pancreatic β-cells, there will be a proportionate increase in glucose entry when blood glucose concentration rises. Glucose is converted into pyruvate and subsequently acetylated, increasing cytosolic adenosine triphosphate (ATP) concentration. The increased ATP concentration binds to and closes potassium ion channels. Reduced efflux causes slight depolarization that opens voltage-sensitive calcium ion channels. An increase in calcium concentration stimulates exocytosis of insulin-containing vesicles (Lodish et al. 2013).

When insulin is circulated throughout the bloodstream, it binds to insulin receptors on cells, which results in an increase in glucose uptake. Insulin binds to specific tyrosine kinases at α-chains, causing receptor dimerization of extracellular domains via disulfide bonds. Subsequent cross-phosphorylation of intracellular β-chains stimulates cross-phosphorylation of intracellular tyrosine residues. Three tyrosine residues have been identified on β-chains being involved in an activation loop. Phosphorylation assumes a conformation apart from a newly-formed catalytic cleft and because of this conformational change, a specific rotation is required to bring catalytic residues closer together and open the cleft for binding substrates of intracellular proteins (Lodish et al. 2013).

Most substrates recruited to the insulin receptor within the cell have an SH2 domain; however, the insulin-receptor substrate (IRS, which does not have an SH2 domain) is also recruited. Autophosphorylation of IRS and SH2 domain-containing proteins creates docking sites for other SH2 domain-containing proteins and phosphotyrosine binding (PTB) domains. The initial recruitment of IRS-1 and IRS-2 provides binding sites for several proteins and activates many pathways via

phosphorylation (Karp 2010). IRS proteins recruit phosphatidylinositol 3 kinase (PI3K), which converts PIP2 to PIP3 and causes phosphorylation of Akt. Akt phosphorylates AS160 and suppresses GAP activity, which then leads to an increase in GTP-bound Rab proteins that facilitate GLUT4 translocation to the membrane (Dash et al. 2009; White 2003; Chang et al. 2004).

Several transduction pathways are either directly or indirectly regulated by insulin stimulation. PKB-β (Akt2) has a primary role in insulin signaling, as its depletion causes a decrease in insulin responsiveness and glycogen synthase kinase-3 activity (GSK3) (Jiang et al. 2003). Further, insulin-signaling components are rapidly activated. Aerobic exercise increases glucose uptake and GSK3 activity, and hyperinsulinemia upregulates IRS-1 and PI3K activity (Worjtaszewski et al. 2000).

In short, insulin promotes glucose uptake in healthy individuals, stimulating its conversion into a more efficient means of energy storage such as glycogen or lipids (Samuel and Shulman 2012). However, there exist several conditions in which insulin sensitivity is attenuated, altered, or dysfunctional altogether. TIIDM is a common example of this phenomenon, and is characterized by a reduction in the responsiveness of target cells, known as insulin resistance (Campbell and Reece 2005). An individual resistant to insulin has impaired transport of GLUT4 to the membrane (Karp 2010).

TIIDM can occur when the insulin receptor becomes resistant to insulin, which can cause defects in insulin signaling pathways. Insulin resistance is a common, yet complex disorder of the endocrine system that is characterized by defective receptor signaling or overstimulation of receptors, yielding hyperglycemia (Bornfeldt and Tabas 2011). Risk factors for insulin resistance are dynamic, but these factors are frequently

associated with obesity and sedentary lifestyle (Karp 2010). As the occurrence of obesity and sedentary lifestyle remains high, insulin resistance manifested as TIIDM has become a public health concern. By the year 2020, it is estimated that there will be 250 million cases worldwide, and by the year 2050, it is estimated that one in three Americans will have TIIDM (Shulman 2000; Samuel and Shulman 2012). Insulin resistance is commonly present 10-20 years before an official diagnosis of TIIDM, meaning there is impairment in insulin signaling and glucose uptake many years before any treatment plan is started.

Physical activity decreases the risk for diabetes. It has long been known that aerobic exercise training improves insulin sensitivity (Medeiros et al. 2010; Wojteszewski et al. 2000). Along with alterations in diet, aerobic exercise might be one of the best natural remedies against insulin resistance; and while genetic predispositions to diabetes might exist, lifestyle modifications greatly reduce these risks.

Profiles during a hyperinsulinemic clamp showed gene expression in skeletal muscle with 284 genes down-regulated and 478 genes up-regulated (Figure 4). Further, 29% of genes affected were involved in translational or transcriptional regulation, indicating a major role of insulin in regulation of protein expression (Rome et al. 2003).

Fourteen percent of transcriptional genes responsive to insulin were involved in energy metabolism, and 12% of the genes were involved in intercellular signaling (Rome et al. 2003). There are dynamic and complex roles for insulin in many signaling pathways. An individual resistant to insulin may exhibit altered transcriptional and translational regulation. Insulin resistance may alter gene expression involved in translation, transcription, and energy metabolism. Deconditioning, which is defined as neglecting physical activity, leads to a reduction in gene expression for insulin and

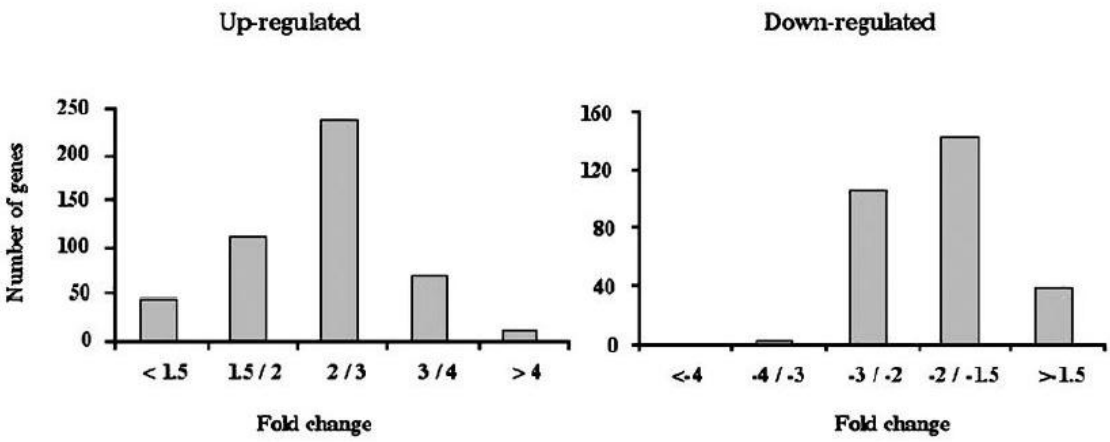

Figure 4: Distribution of fold change in mRNA levels induced by insulin in human skeletal muscle (Rome et al. 2003). This figure shows almost 250 genes having a 2-3 fold increase in expression upon insulin stimulation. In addition, there appears to be almost 140 genes with a -1.5 to -2 fold decrease in expression upon the same insulin stimulation. Insulin has a dynamic impact on gene expression and appears to modify the expression of 762 genes.

adipocytokine signaling. Gene expression for these categories were up-regulated in physically conditioned muscle, suggesting that physical activity plays a role in the diabetes (Lammers et al. 2012).

Muscle Glucose Uptake

Skeletal muscle glucose uptake is dynamic, but often it is distinguished by three phases: an extracellular component, and transport component, and an intracellular component (Figure 5). The interaction of these physiological mechanisms regulate glucose uptake into skeletal muscle (Wasserman and Ayala 2005).

The extracellular component relates increased blood flow to an increase in substrate delivery to the cell. In mice treated with sildenafil + L-arginine, which acts as a vasodilator, glucose uptake was significantly greater in soleus and gastrocnemius muscle tissues as compare to mice treated with a control vehicle (Ayala et al. 2007). This suggests an important role in glucose delivery to muscle tissue in the bloodstream.

The transport component of glucose uptake indicates the importance of GLUT4 translocation to the membrane for adequate glucose uptake. GLUT4 knockout mice were observed to have significantly less insulin-stimulated glucose uptake than control mice (Stanford and Goodyear 2014). Further, there appears to be an exercise component regulating GLUT4 translocation for glucose uptake. During an acute bout of exercise, mice lacking the insulin receptor were observed to have similar glucose uptake to mice with intact insulin receptors (Stanford and Goodyear 2014). Individuals with TIIDM experience a reduction in blood glucose concentrations during acute bouts of exercise because of exercise-induced glucose uptake (Rose and Richter 2005). Together, these

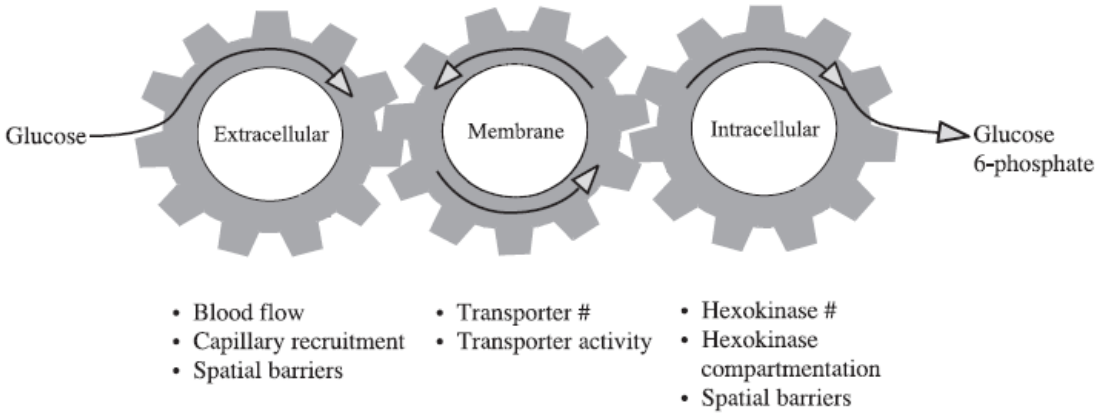

Figure 5: Interaction of physiological mechanisms in control of muscle glucose uptake (Wasserman and Ayala 2005). The first component involves substrate delivery to the cell, known as the extracellular component. The second component involves glucose transport from extracellular spaces into the cell, known as the membrane component. The final component involves hexokinase phosphorylation of glucose to maintain its presence in the cell, known as the intracellular component. Any of these steps can be rate-limiting in glucose metabolism.

data support the need for GLUT4 in facilitating glucose transport across the cell membrane.

Finally, the intracellular component indicates the need for glucose to be phosphorylated by hexokinase-II, an enzyme initiating the first step in glycolysis. Glycolysis then catabolizes glucose into useable products for energy production (Rose and Richter 2005).

Any component in skeletal muscle glucose uptake may be rate-limiting; however, investigators generally agree that transport activity of glucose across the membrane is the most common rate-limiting step (Figure 6). The transport of glucose depends on GLUT4 translocation through insulin-stimulation or exercise-mediated mechanisms (Stanford and Goodyear 2014). Insulin resistance is observed in skeletal muscle tissue as a reduction in glucose uptake into the cell, further supporting that transport activity is a common rate-limiting step (Rose and Richter 2005).

Modern Exercise Physiology in Medicine: New Models for Discovery

Exercise has long been known to have several health benefits. As part of a health treatment plan, exercise is associated with positive health outcomes and sedentary behavior is associated with a reduction in positive health outcomes (Bamman et al. 2014; Thyfault and Krogh-Madsen 2011). Further, aerobic exercise is associated with an increase in or maintenance of working levels of aerobic capacity (Gaesser and Rich 1984; Pollock et al. 1987). In addition, exercise is linked to improved insulin sensitivity and has been shown to reverse impairments in glucose uptake observed in TIIDM (Lessard et al. 2011; Medeiros et al. 2010). Sedentary behavior is linked to an increased risk of

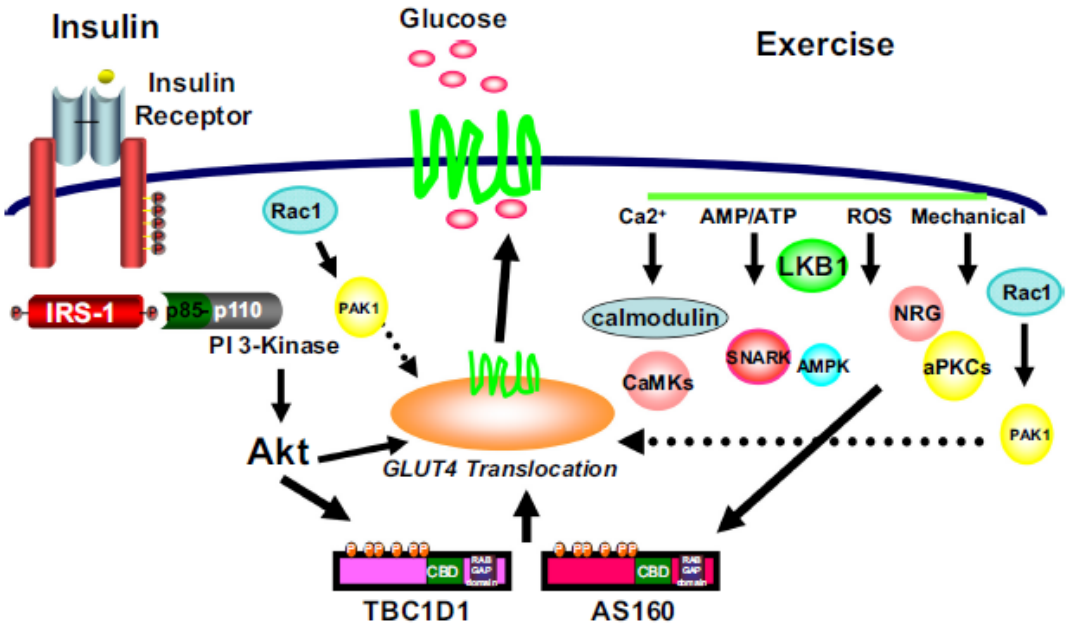

Figure 6: Molecular mechanisms regulating glucose uptake in skeletal muscle (Stanford and Goodyear 2014). Scientific investigators suggest glucose membrane transport is rate-limiting in insulin resistance. GLUT4 translocation to the membrane is needed for glucose uptake into the cell. On the left, the figure shows insulin binding to its receptor and recruiting IRS-1, which then recruits PI3K. This recruitment allows phosphorylation of Akt, which is required for insulin-stimulated GLUT4 translocation. On the right, the figure shows plausible means of exercise-stimulated glucose uptake via GLUT4 translocation to the membrane. Stanford and Goodyear postulate Ca^{2+} and calmodulin are primarily responsible for exercise-stimulated glucose uptake. Studies support a lack of skeletal muscle glucose uptake in GLUT4 knockouts.

developing TIIDM (Hamilton et al. 2014). From these data, exercise appears to increase the likelihood of good health while decreasing the risks for poor health. But to fully understand the impact of exercise on health and to what extent it aids in cellular physiology, it may be helpful to review some history in exercise physiology.

Exercise physiology has been applied for years, but the discovery of heat production in muscle in 1920 is where modern exercise physiology really established its roots. In this experiment, heat production was characters at different phases of muscle contraction, relaxation, and recovery (Hill and Hartree 1920). Much of the heat production was anaerobic, which then began investigation on what is now known as aerobic and anaerobic metabolism (Hartree and Hill 1923).

A.V. Hill was a long-distance runner and noticed what appeared to be a maximum level of oxygen consumed by himself and other athletes during bouts of exercise (Hill et al. 1924). From these observations came the term "VO_2 max," which was later described as the maximum amount of oxygen taken up by the body at peak levels of physical exertion. At this level, any increase in physical exertion does not elicit an increase in oxygen consumption (Hill et al. 1924).

In 1977, data were published suggesting mitochondrial adaptations in response to exercise (Figure 7). In this study, athletes were trained for eight weeks at 45% of VO_2 max with muscle biopsies taken each week. After three weeks of training, both oxidative and glycolytic enzymatic activity increased in addition to working aerobic capacity. These adaptations were reversed after two weeks of detraining (Henriksson and Reitman, 1977). These data support exercise benefits at the cellular level and suggest a reversal of these benefits is associated with physical inactivity.

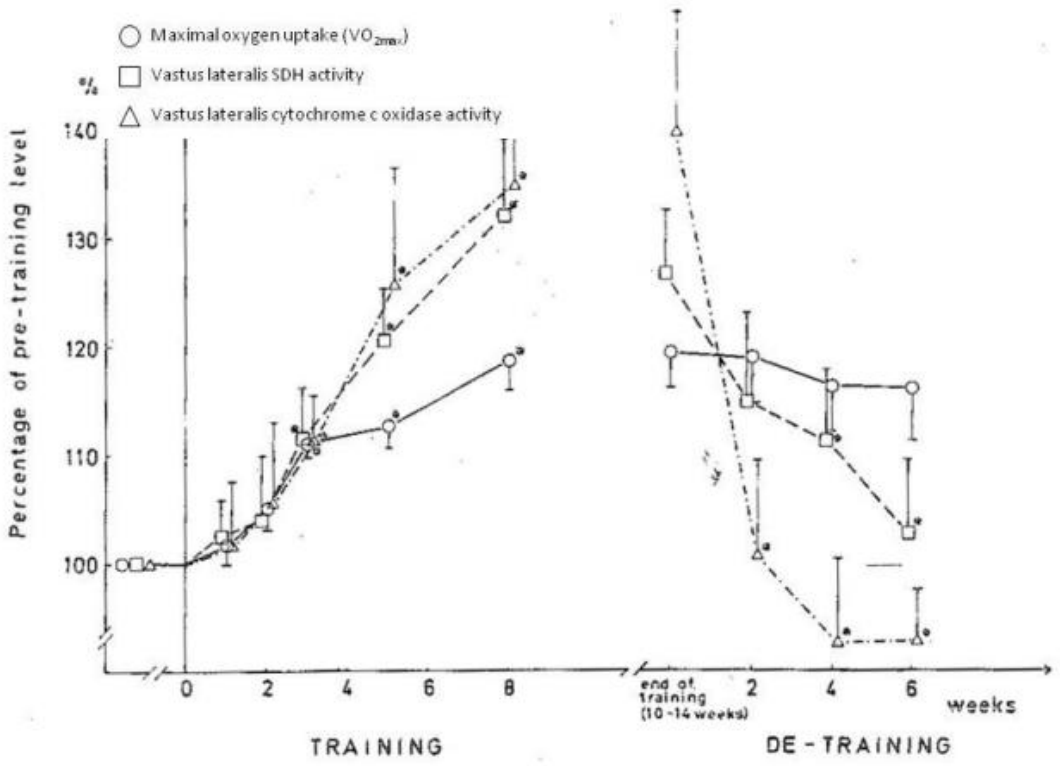

Figure 7: Time course for changes in two mitochondrial enzymes and VO_2 max during training and detraining (Henriksson and Reitman 1977). The left panel shows the effect of training on enzymatic activity. After three weeks of training, there begins to be an increase in oxygen uptake, succinate dehydrogenase (SDH) activity, and cytochrome c oxidase activity. At the conclusion of 8 weeks, there are significant increases in all three measures. The right panel shows the effect of detraining or physical inactivity on enzymatic activity. After six weeks of detraining, there are significantly lower levels of SDH activity and cytochrome c oxidase activity.

Aerobic capacity refers to a working percentage of VO_2 max and is implicated by a component of time. Thus, exercise training might increase the duration of a high working percentage of VO_2 max due to skeletal muscle mitochondrial adaptations and increased cardiorespiratory fitness (Bruce 1984). Studies consistently link high aerobic capacities with increased longevity and increased overall health; however, it has not been easy to test the effect of aerobic capacity on different health outcomes due to many external factors, such as training (Koch et al. 2012). In 2005, a study was published on two lines of rats contrasting for aerobic capacities based on an endurance run to exhaustion (Figure 8). From an NIH stock of rats, these rats were run on a treadmill at 15% and 6 m/min until exhaustion. Rats running furthest were selected to breed together, beginning the high endurance running capacity (HCR) group to mimic high aerobic capacity. Rats running the least were selected to breed together, beginning the low enduring running capacity (LCR) group to mimic low aerobic capacity (Wisloff et al. 2005).

This rat model has been used in many countries and provides an unbiased model to assess the impact of aerobic capacity on different health outcomes (Koch and Britton 2005). As mentioned before, high aerobic capacity is consistently linked with positive health outcomes and increased longevity in an unbiased rat model (Figure 9). Further, VO_2 max has been used consistently as a measure of cardiorespiratory function and potential, which regulates oxygen delivery for cellular energy production (Timson et al. 2008).

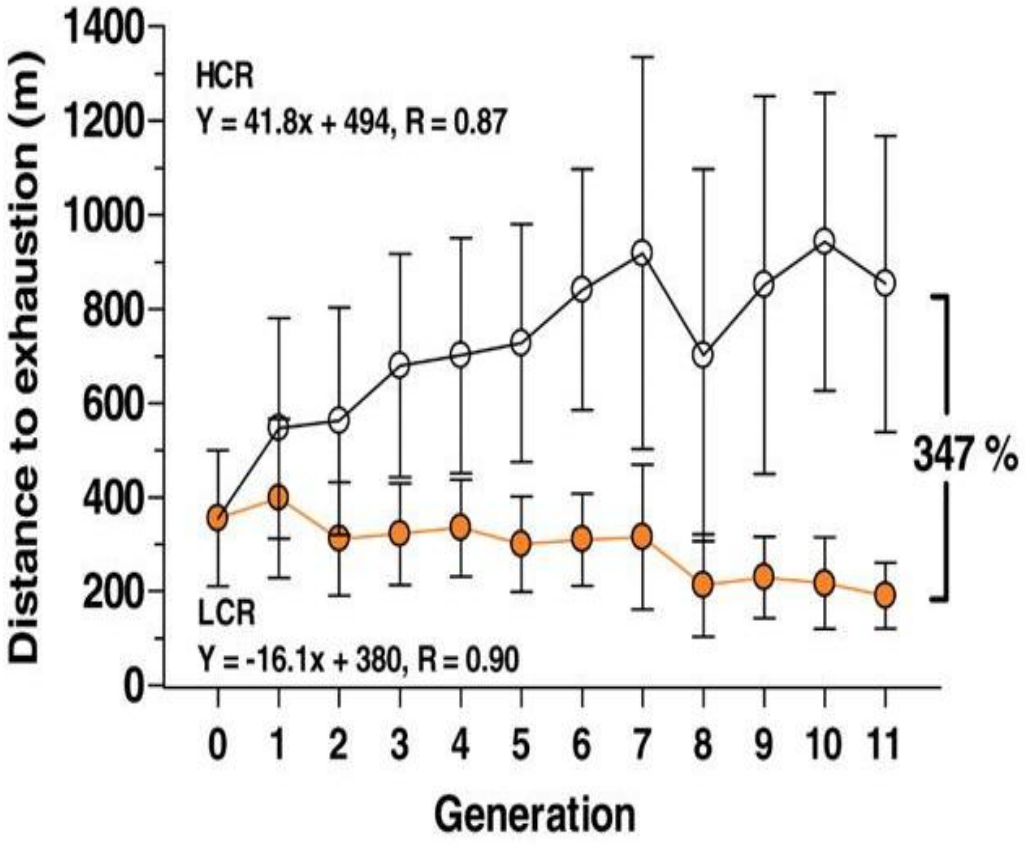

Figure 8: Generation 0-11 of rats selected for low and high intrinsic endurance running capacity (Wisloff et al. 2005). After six generations, a significant difference was observed in endurance running capacity and after 11 generations, the difference in endurance running capacity was 347%. Endurance running capacity is an indirect measure of functional aerobic capacity.

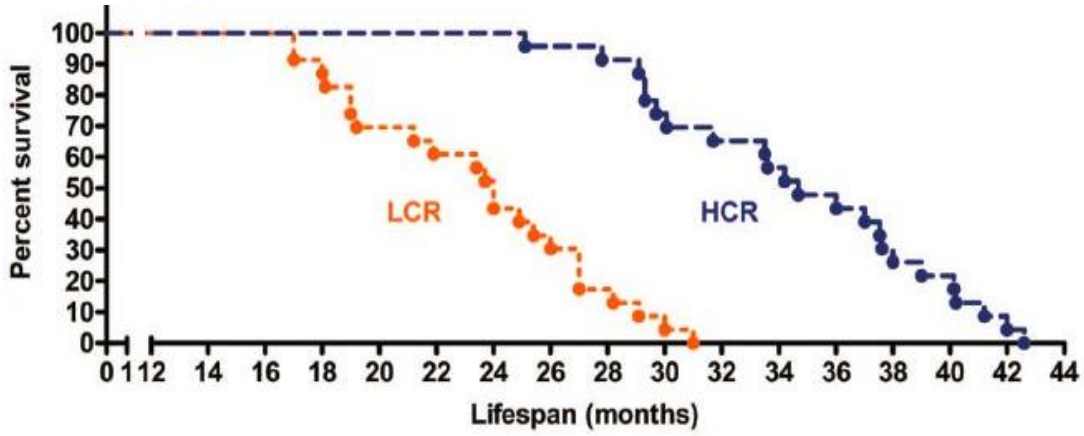

Figure 9: A prospective test of the "aerobic hypothesis" in rats selectively bred to contrast for intrinsic endurance exercise capacity (Koch et al. 2011). This figure highlights lifespan of LCR and HCR rats at generation 14. The median life expectancy of LCR rats was 24.0 months whereas HCR rats had a median of 34.7 months ($p<0.001$).

Aerobic Capacity in LCR and HCR Rats

VO_2 max is a measure of the maximum amount of oxygen taken up by the body at peak levels of physical exertion. At this level, any increase in physical exertion maintains the same oxygen consumption in the body. Oxygen is essential for aerobic organisms as its utilization is required for adenosine triphosphate (ATP) production during oxidative phosphorylation. Oxygen is reduced in the electron transport chain and therefore able to accept electrons via redox reactions in mitochondrial membranes. This transfer of electrons through different complexes helps to generate energy for the inner mitochondrial membrane to pump protons across its membrane and subsequently generate potential energy via a pH gradient. As protons flow back across the gradient to reestablish proton concentration equilibrium, there is production of ATP as these protons cycle through ATP synthase (sometimes called Complex V). This coupled process of chemiosmosis provides considerable amounts of energy production for cellular functions (Lodish et al. 2013). Therefore, oxygen metabolism and energy transfer govern intrinsic aerobic capacity.

As organisms evolved, the presence of oxygen within cells has increased energy transfer 18-fold (Koch and Britton 2005). This improvement in energy transfer may have facilitated increased survival and lifespan. Data support many diseases are a direct result of defective mitochondria or impairments in mitochondrial oxidation/detoxification pathways (Koch and Britton 2005). A high aerobic capacity is consistently linked with increased longevity in unbiased rat models. The increased ability to consume and utilize oxygen is directly related to survival in this model, as low aerobic capacity has

demonstrated increased risks for conditions related to early morbidity. Known as the "aerobic hypothesis," a large reduction in the energy transfer of oxygen is central to complex disease phenotype and aging in rats (Koch et al. 2011).

Whereas intrinsic aerobic capacity is primarily regarded as a genetic trait, there are environmental interventions to increase aerobic capacity and subsequently increase physical fitness levels (Koch and Britton 2005). Exercise is the intentional maintenance of some component of physical fitness (Caspersen et al. 1985). Many US individuals take no measures in maintaining or increasing components of fitness (Physical Activity, Figure 1).

Low aerobic exercise capacity has potential to increase the risk of certain mortality-related diseases, an theory known as the "aerobic hypothesis" (Koch et al. 2011). With these observations, low aerobic capacity may be associated with a reduction in insulin sensitivity. Hoydal and colleagues state that within an established line of artificially selected high and low-aerobically conditioned rats, the rats of low aerobic capacity portrayed greater insulin resistance (Hoydal et al. 2014).

Aerobic exercise is associated with increases in functional aerobic capacity (Short et al. 2003). Insulin signaling and glucose transport *ex vivo* is lower in rats artificially bred for low-aerobic capacity as compared with high-aerobic capacity rats. In skeletal muscle, aerobic exercise training increases aerobic capacity and reverses many impairments to glucose metabolism (Lessard et al. 2011). While a correlation between physical activity and insulin signaling may exist, it remains unclear whether physical activity and aerobic capacity regulate insulin signaling *in vivo*.

AKT (Protein Kinase B) of the Insulin Signaling Pathway

Phosphorylation of protein kinase B (PKB or Akt) is a common measure of functional insulin signaling (Manning and Cantley 2007). Insulin-mediated activation of Akt gives stimulates translocation of the GLUT4 vesicle to the plasma membrane for glucose uptake (Gonzales and McGraw 2009). Akt has been demonstrated to be required for appropriate GLUT4 translocation to the membrane and to maintain glucose homeostasis. Further, insulin signaling is often measured indirectly as a function of protein kinase activation by probing for phosphorylated Akt (Ser^{473}) and its associated substrates (Lessard et al. 2011).

Akt is a versatile protein kinase and an important signaling node in higher eukaryotic cells. Its abundance throughout all cell types renders its central role in regulation of human physiology and complex disease. (Manning and Cantley 2007). Akt exists in three isoforms (Akt1, Akt2, and Akt3), each with unique functions and likely subcellular specificity. Akt1 is the most prevalent isoform in endothelial cells and functions in angiogenesis and cell growth. This is made evident as Akt1 knockout mice do not grow to be as large as wilder-type counterparts, which is possibly due to the ability of Akt to activate endothelial nitric oxide synthase via phosphorylation of S1177, therefore increasing vascular remodeling and vasodilation consistent with angiogenesis and growth (Manning and Cantley 2007; Gonzalez and McGraw 2009).

Akt2 is the most prevalent isoform in tissues that are sensitive to insulin. Its activation stimulates GLUT4 translocation to the plasma membrane (Manning and Cantley 2007). Akt2 knockout mice manifest impairments in glucose utilization similar to that of Type-II diabetes mellitus (Gonzales and McGraw 2009). Hypotheses have been

made suggesting that insulin will preferentially accumulate Akt2 in insulin-sensitive tissues, over other Akt isoforms, to the plasma membrane. Although this might be true, the mechanism for this observation is not clear (Gonzalez and McGraw 2009).

Finally, Akt3 is thought to function in neuronal development as Akt3 knockout mice show impairments in early brain development (Gonzalez and McGraw 2009). Recent data suggest a link between insulin resistance and cognitive impairment (Biessels and Kappelle 2005; Liu et al. 2011; Ferreira et al. 2014). Insulin is known to play some kind of role in learning, memory, and neuromodulatory functions (De Felice et al. 2014).

In summary, there exists an unidentified mechanism linking diabetes, obesity, and physical inactivity. A common phenomenon observed in each condition is reduced insulin sensitivity (Dwyer-Lindgren et al. 2013; Shulman 2000; Tremblay and Wilms 2003). Physical inactivity is associated with reductions in insulin sensitivity, and sedentary behavior has been consistently linked to poor health outcomes. Conversely, physical activity has demonstrated reversal in metabolic impairments and has been consistently linked to positive health outcomes (Medeiros et al. 2010; Lessard et al. 2011; Koch et al. 2009). Appropriate insulin signaling is crucial to maintain energy metabolism (Campbell and Reece 2005). Exercise is an intentional form of physical activity with the intention of improving physical fitness, and exercise may result in skeletal muscle metabolic adaptations which are reversed due to physical inactivity (Caspersen et al. 1985; Henriksson and Reitmann 1977). These adaptations may help increase functional levels of aerobic capacity (Henriksson and Reitmann 1977). High aerobic capacity is associated with increased health and longevity in rat models, with data suggesting insulin resistance in LCR rats *ex vivo* as compared to HCR rats (Koch et al. 2009; Lessard et al.

2011). Together, these data and observations may support a link between low aerobic capacity and reductions in insulin sensitivity which manifest through insulin signaling protein expression.

Hypotheses

My hypotheses were as follows: 1) Low aerobic capacity is associated with reduced whole-body insulin sensitivity in a conscious, unrestrained rat and 2) Low aerobic capacity is associated with reductions in Akt signaling in slow, oxidative skeletal muscle (soleus).

MATERIALS AND METHODS

Research Compliance

All research compliance training and certification was obtained via CITI modules in October, 2013. This project followed guidelines set forth by both an Institutional Review Board and a Situational Animal Care and Use Committee in the spring of 2014. Animals used in this study were treated according to an approved protocol such that appropriate care and oversight was ensured.

Obtaining and Preparing Rat Cohorts

Aerobic capacity is a predictor of mortality and strongly associated with longevity (Koch et al. 2012). Further, aerobic exercise has been shown to reduce insulin resistance (Medeiros et al. 2010). Together, these observations imply that aerobic capacity might play a role in insulin resistance and might be associated with a type-II diabetes mellitus phenotype.

The selection process began with a founder population of heterogeneous N:NIH rats (n=168). Through an inclined run to exhaustion, investigators ascertained intrinsic aerobic capacity since a relationship exists between running velocity and oxygen consumption (Koch and Britton 2001). Rats running farthest were selected to breed together to begin the high aerobic capacity line; rats running the least amount were selected to breed together to begin the low aerobic capacity line. To maintain genetic variation, a rotating cycle of 13 rat families was scheduled to keep the rate of inbreeding less than 1%, which also helped reduce environmental variance (Koch and Britton 2005).

Divergent lines became significantly apparent within 6 generations (Koch and Britton 2001). After 11 generations, there was observed to be a 347% difference in running capacity, suggesting there may be a difference in intrinsic aerobic capacity (Wisloff et al. 2005). Using this rat model, both genetic and environmental influences affecting aerobic capacity and cellular physiology can be examined (Koch et al. 2012).

To test the hypotheses listed above, LCR and HCR rat cohorts following 34 generations of selective breeding were obtained from the University of Michigan. HCR rats ran further than LCR rats, suggesting an intrinsic difference in aerobic capacity, $p<0.001$ (Figure 10). Fourteen HCR rats and fourteen LCR rats were used in this study beginning in April, 2014. Rats were housed singly, maintained on a 12-hour light/dark schedule, and acclimated for least two weeks upon arrival.

Body Mass and Food Consumption

Body mass measurements and food consumption measurements were made once per week throughout the duration of survival studies. Rats were massed in a tared container on an electronic triple beam balance. Food mass for each week was measured in a tared container on an electronic triple beam balance. Data were plotted in excel spreadsheets and graphs were made to observe change in mass over time. In addition, transformed data were obtained by dividing the mass of food consumed each week by the average body mass for each week. Data included in this project reflects results after 12 weeks of data collection. After 12 weeks, LCR and HCR rats were sub-divided to one of four groups for *in vivo* data collection.

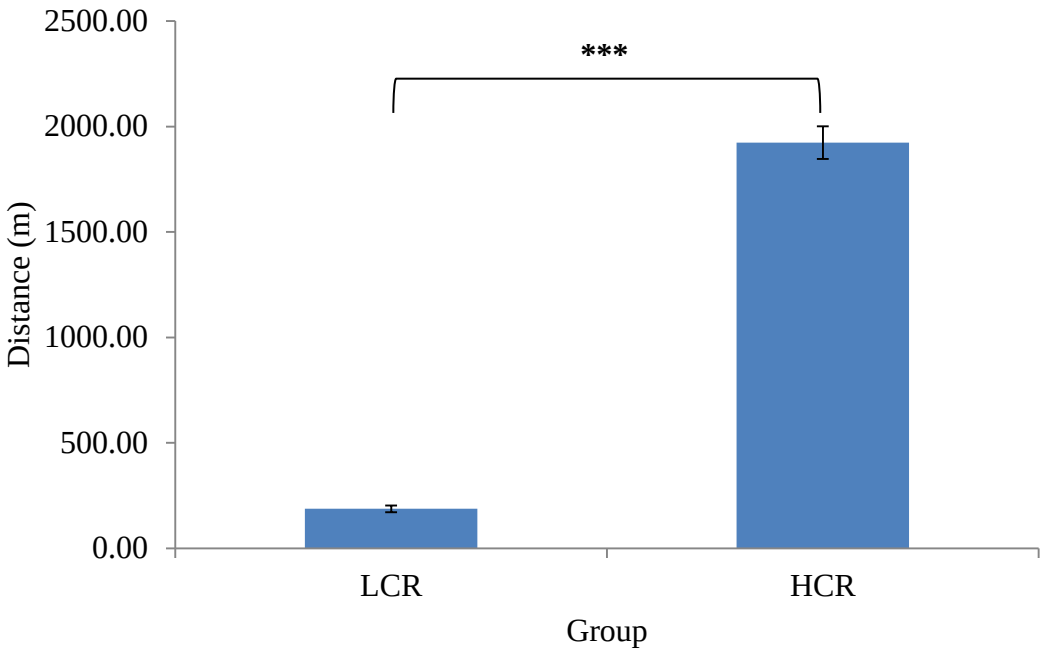

Figure 10: Running distance to exhaustion of HCR and LCR rats obtained from University of Michigan after 34 generations. Endurance running capacity is a good indication of intrinsic aerobic capacity. The HCR rats on average ran 10X further than LCR rats ($p<10^{-17}$). The difference in intrinsic aerobic capacity manifests with this initial treadmill running test to exhaustion, ***$p<0.001$.

Group Assignments

To determine the impact of aerobic capacity on insulin sensitivity and insulin signaling, LCR and HCR rats were divided and weight-matched into one of two groups: basal (B) or insulin-stimulated (IS). Rats in the IS group were catheterized and clamped, as described below. Rats in the B group underwent a similar, sham surgery. The final groups were as follows: LCR-B (*n*=7), LCR-IS (*n*=7), HCR-B(*n*=7), and HCR-IS (*n*=7). Since surgery survival was not 100%, the final groups used in the analysis were as follows: LCR-B (*n*=4), LCR-IS (*n*=3), HCR-B (*n*=7), and HCR-IS (*n*=5). Groups were assigned based on body mass at week 12 so there was no difference between groups within LCR and HCR cohorts.

Mouse Antenna for Sampling Access (MASA) Production

The MASA is a device constructed to isolate and secure intravenous catheters on the back of a rat necks for placement, sampling, and ease of access to catheter tubing. MASA construction included silicone medical adhesive, Tygon 0.02”x0.06”x0.02” tubing (Fisher Scientific), 0.132”x0.183” tubing (Fisher Scientific), and 22G blunt hypodermic tubing. Twenty-two gauge blunted needles were used for connecting the MASA to the catheters.

First, 1 ½ 22G needles were blunted on two sides using a file and pliers to a needle length of 24.0 mm. Then, two pieces of 0.02”x0.06”x0.02” tubing were cut to lengths of 50.0 mm. One piece of tubing was colored red and designated for the arterial line while the other tubing was colored black and designated for the venous line. These tubes were each connected to blunted, 22G needles. After tubing was connected to

blunted needles, the needles were bent to a 135^{o} angle and positioned 45^{o} from each other . A 22.0 mm piece of 0.132”x0.183” tubing was cut and placed over the two smaller tubes so the red tubing was on the left when the needles were pointing away (This would ensure the red tubing was always assigned to the left carotid artery per surgery protocol). Finally, silicone adhesive was placed on a plastic weigh boat and the MASA was placed in the adhesive and adjusted for desired formation. All MASAs were autoclaved and prefilled with 10 mU/mL heparinized saline prior to use in surgery. Final angle measurements, lengths, and placement varied as each MASA was customized to fit each rat in surgery.

Carotid and Jugular Catheterization

Under guidance from Missouri State University’s veterinarian and IACUC panel, surgery protocol was approved and practiced on Sprague-Dawley rats before beginning LCR and HCR surgeries. LCR-IS (n=7) and HCR-IS (n=7) underwent a catheterization procedure as described by Ayala et. al (2011) to include the left carotid artery and the right jugular vein. The surgery required the following sterile instruments: 10 cm straight, serrated, extra fine Graefe forceps (FST by Dumont), 10 cm curved, serrated, Graefe forceps (FST by Dumon), 3 mm straight Vannas spring scissors (LaCrosse Stainless), 10 cm sharp Iris scissors (LaCrosse Stainless), 12.5 cm Halsey micro needle holder, 12.5 cm straight and smooth ultra-fine Hemostat (FST by Dumont), serrated Adson forceps (FST by Dumont), and 2 teeth curved Iris forceps. The body mass of each rat was taken prior to surgery preparation so antibiotic injection could be calculated. The surgical table was sterilized with 70% bleach followed by 70% isopropanol, and bench guards were taped

down prior to surgery. A heating pad was set on low and a sterile, surgical drape was taped over the heating pad. Finally, the anesthesia nose-cone was placed on one end of the surgical field and taped down. A surgical tray was sanitized with 70% ethanol, as were all surgical instruments prior to surgery. The tray was then filled with 1 part cyclohexamide to 200 parts cool water with all surgical instruments placed inside the surgical tray until needed.

Rats were placed in chamber pre-filled with 3-4% isoflurane anesthetic gas. Upon anesthetization, rats were transferred to the surgical field with the nose placed in the nose-cone for continuous oxygen/anesthesia administration throughout surgery. The rat was prepared for surgery by shaving the neck from the chin to the xiphoid process, and outward to the shoulder. Claws were clipped and puralube ophthalmic ointment (Dechra) was applied. The rat was flipped and shaved from the base of the skull to the shoulderblades, and outward to the sides of the neck. After the rat was prepared for surgery, the rat was raised off the surgical drape and a new, sterile drape was placed between the rat and the heating pad. Preparation continued with application of betadine solution to recently shaved areas. Extremities were taped down before placing a sterile drape over the rat.

A small, midline incision was made from the hyoid to the middle of the base of the sternum. Tissue was blunt-dissected to expose the sternomastoid muscle on the left side of the rat. The muscle was reflected to expose the left carotid artery and extra tissue was teased off the artery. Before isolation of the artery, it was important to isolate the vagus nerve away from the artery. After the artery was isolated with forceps, the artery was tied off with silk suture (Fine Science) at the cephalic end and a loose knot was tied

at the caudal end. A small incision was made in the artery for insertion of a sterile, beveled catheter which was prefilled with 10 mU/mL heparinized saline. This catheter was tied securely to the artery and patency was tested using a syringe and blunted needle for catheter access before clamping the catheter with a sterile pin.

On the right side of the rat, tissue was teased until the jugular vein was isolated. The vein was tied at cephalic and caudal ends as previously described and a small incision was made. A sterile, beveled catheter was prefilled with 10 mU/mL heparinized saline before placement into the jugular vein. The catheter was tied securely before testing patency with a syringe and blunted needle attached to the catheter. After patency was ensured, the catheter was clamped with a sterile pin.

When both lines were patent, the rat was flipped dorsally to expose the back. A small incision was made between shoulder blades extending from the base of the skull. A blunted needle was tunneled from the ventral incision around both sides of the neck to the interscapular incision made on the back. The catheters were threaded through the blunted needle such that the catheter placement in the front of the body resulted in catheters being run out the dorsal incision.

The MASA was placed in the interscapular incision. Blunted needles extending from the MASA were custom-bent to fit the incision and meet the catheters. The carotid line in the MASA was clamped, cut to desired length, and attached to the MASA. The jugular line in the MASA was clamped, cut to desired length, and attached to the MASA. Patency was confirmed after unclamping the MASA by using syringes and blunted needles to draw up blood. A lock solution of 50 mU/mL heparinized saline in 10% glycerol was inserted in the MASA lines to reach into the catheters.

Antibiotic and pain-relieving injections were administered. Medications consisted of Metacam (0.15 mg/kg), Baytril antibiotic (10 mg/kg), and 3.0 mL saline subcutaneous injections.

Incisions were closed with nylon suture and 2% mupirocin ointment (Dechra) or Neosporin (Johnson & Johnson) was applied to the incision. Lidocaine ointment (Taro Pharmaceuticals) was applied on and around the sites of incision for pain relief. The rat was given oxygen for a short time until observed to slightly regain consciousness, when the rat was transferred to a clean cage for recovery. The cage was half-placed on a heating pad for 24 hours to aid in the recovery process, with food and water available at all times. Each day the body weight was monitored in addition to overall wellbeing. Rats were deemed unsuccessful in surgery if the body mass dropped more than 20% from pre-operative body mass or if overall appearance did not seem healthy (such as staggered breathing or foaming at mouth).

Daily post-operative care included testing catheter patency and flushing catheters with heparinized saline solution. Observations and care included measuring body mass, applying antibiotic ointment, and making notes about the overall health and appearance of the rat. Rats were allowed to recover at least 5 days and no more than 7 days before performing a metabolic clamp procedure (as described below). Other materials used but not previously mentioned are trimmers, sterile boxes, gauze, cotton swabs, sterile saline solutions, and other sterilized surgical instruments as needed.

Euglycemic-Hyperinsulinemic Clamp

A euglycemic-hyperinsulinemic clamp was performed to measure insulin sensitivity (Ayala et al. 2011). This procedure involved a steady infusion of insulin while altering glucose administration until a target value of blood glucose concentration was obtained (Figure 11). Literature suggests a clamped value of blood glucose concentration to be 130 mg/dL. This procedure allowed for accurate measurement of blood glucose concentration and determination of insulin sensitivity (Tam et al. 2012). This clamp procedure provided a good way to measure insulin sensitivity and therefore define an insulin-resistant phenotype commonly manifested in TIIDM.

Rats fasted 5 hours prior to the clamp procedure, where t=0 min refers to the time immediately following the conclusion of the fast. Rats in B groups began fasting 1 hour prior to rats in IS groups. This allowed for time to euthanize a rat from the B group and harvest tissues in the same day before beginning the clamp procedure for an IS rat. All rats were massed prior to fasting so calculated values of 0.25 mU/μL insulin administration could be made to infuse at 4 mU/kg/min. Insulin was made using 50.0 μL of 100 U/mL insulin (Novolin) placed into 20.0 mL 3.0% albuminized saline (600.0 μL plasma in 19.4 mL saline). Glucose was purchased as a 50% dextrose solution. The arterial line used for blood sampling was prefilled with 10 U/mL heparinized saline, while the glucose and insulin lines were prefilled with respective solutions. The glucose and insulin lines were connected via a y-connector to provide steady infusions of each into the jugular line.

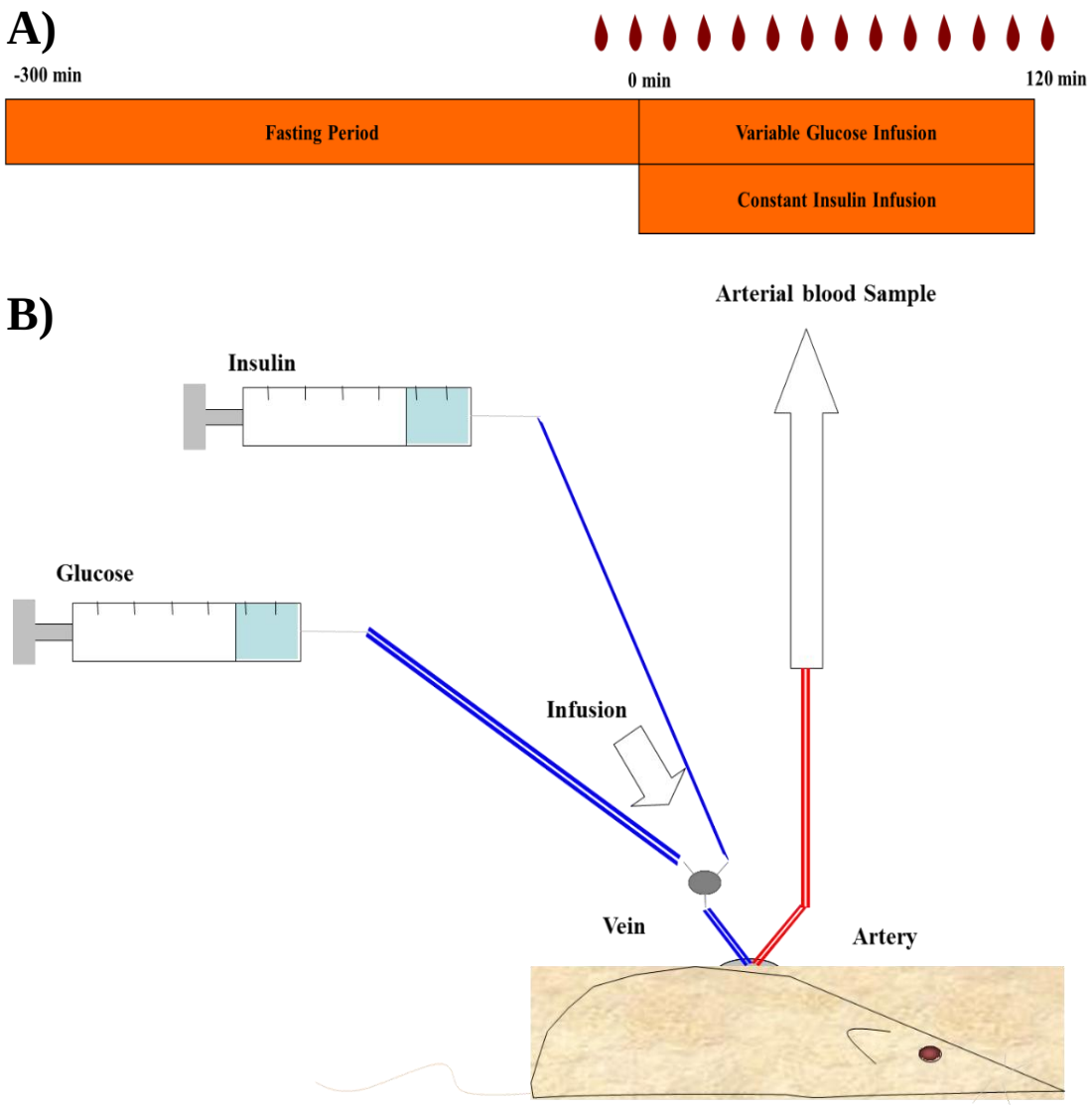

Figure 11: Experimental design for the euglycemic-hyperinsulinemic clamp procedure. Panel **A)** shows the time layout from the beginning of the fast (t=-300 min.) to the infusion of glucose and insulin (t=120 min.). Insulin was infused constantly at 4 mU/kg/min whereas glucose was infused at variable rates so as to plateau blood glucose concentration at 130 mg/dL. The red blood droplets indicate blood glucose readings that were taken every 10 minutes during the metabolic clamp procedure. Panel **B)** displays the setup of insulin and glucose infusion pumps into the jugular vein of a catheterized rat and blood sampling access from the carotid artery.

IS rats were connected to the arterial sampling line and jugular infusion line two hours prior to the start of the clamp procedure to acclimate to the setup so the procedure accurately reflected results of insulin sensitivity in a conscious, unrestrained rat.

The first blood sample was taken at t=-10 min for a baseline reading to ensure the rat was not hypoglycemic and also to set an initial glucose infusion rate. A small sample of blood was taken in a capillary tube for hematocrit reading. Insulin was administered via the infusion pump just seconds before glucose so activation of signaling pathways would prevent hyperglycemia. Blood glucose readings were taken at t=0 min and then in 10 minute intervals for the duration of the 2-hour clamp procedure. Fresh arterial blood was drawn from the carotid artery and read on a ReliOn Prime glucose meter with ReliOn Prime blood glucose test strips (Walmart). Blood glucose measurements, along with glucose infusion rates, were recorded throughout the duration of the clamp procedure until the target blood glucose range of about 130 mg/dL was obtained for consecutive readings. After each blood glucose readings, the glucose infusion rate was adjusted in accordance with the reading in attempt to obtain the target reading of 130 mg/dL. At the conclusion of the study, a small sample of arterial blood was taken for hematocrit reading to ensure minimal loss of blood during the study. About 1.0 mL of blood was taken from the arterial line for plasma insulin concentration at t=120 min. All blood samples were taken with heparin-coated syringes and the blood was placed into prelabeled EDTA-coated tubes.

Blood samples were centrifuged for 4 min at 4.0 ^{o}C and plasma supernatant was transferred to 1.5 mL prelabeled microcentrifuge tubes and stored in a freezer at -80.0 ^{o}C until Magpix (Merck) analysis.

After blood samples were taken, rats were anesthetized in a chamber prefilled with 3-4% isoflurane gas so that tissues could be harvesting.

Tissue Harvesting

Immediately following the clamp procedure, insulin-stimulated blood samples were taken from the carotid arterial line of IS rats. IS rats were immediately placed under 3-4% isoflurane gas anesthesia before tissue collection. Rats in B groups were taken from the cage at the conclusion of the 5-hour fast and placed in a chamber prefilled with 3-4% isoflurane gas for anesthetization. Both tissue and blood collection was performed under anesthesia for rats in B groups. Blood samples were taken from B groups via a heart stick prior to tissue collection. Capillary tubes were used to determine hematocrit levels of IS rats both before and after the clamp procedure and analyzed by centrifuging samples and reading on a hematocrit reader.

The surgical table was sanitized and a benchguard taped down before transferring the rat from the isoflurane chamber to the nose-cone administration of gaseous anesthesia. All instruments were sterilized with 70% ethanol along with the surgical tray. The tray was filled with 1 part cyclohexamide to 200 parts cool water and the instruments were placed in the surgical tray for the entirety of tissue harvesting procedures. This ensured sterility as tissues were being harvested.

The gastrocnemius, soleus, plantaris, liver, heart, epididymal fat, mesenteric fat, and brain samples were harvested (Morris) for protein analysis using a 10.0 cm straight, serrated, an extra fine Graefe forceps, and a 10.0 cm sharp Iris scissors. Samples were rinsed in ice-chilled PBS and were dabbed on sterile gauze before being wrapped in

prelabeled aluminum foil and immediately flash-frozen in liquid nitrogen. Samples were transferred to Missouri State University where the samples were stored at -80.0 ^{o}C for future analysis. Brain samples were dissected by Margaret Thornton and Katelyn Moore.

Tissue Homogenization

Forty soleus muscle samples from basal and insulin-stimulated LCR and HCR rats were taken from -80 ^{o}C storage and placed into liquid nitrogen. Muscle mass was recorded in milligrams using an electronic triple beam balance (Mettler Toledo). Samples were again placed in liquid nitrogen following mass measurement. Two 1.50 mL microcentrifuge tubes were labeled for each soleus muscle homogenate and chilled on ice. The Tris-Triton buffer used in the working lysis buffer was comprised of the following materials: 10 mM Tris (pH=7.4), 100 mM NaCl, 1 mM EDTA, 1 mM EGTA, 1% Triton x-100, 10% glycerol, 0.10% SDS, and 0.50% deoxycholete. The working lysis buffer was prepared using 99 µL of the Tris-Triton buffer and 1 µL proteinase inhibitor cocktail (Sigma P8340) per 10 mg of muscle sample. This lysis buffer of 100 µL buffer/10 mg muscle was transferred into a prechilled 10.0 mL glass tube, using a 1000 mL pipet, for muscle tissue homogenization. Muscle tissues were transferred from liquid nitrogen one sample at a time into a mortar that was prechilled in liquid nitrogen. The muscle sample was then crushed using a prechilled pestal until the tissue resembled a powder. The muscle powder was then transferred to the prechilled 10.0 mL glass tube where the sample was lysed using a probe to grind tissue and mix with the lysis buffer. Upon completion of muscle tissue lysis, the homogenate was transferred to 1.50 mL

prechilled and prelabeled microcentrifuge tubes using a 1000 mL pipet with a widened tip for efficient transfer.

When all muscle homogenate had been collected, samples were centrifuged at 4 ^{o}C for 15 minutes and the supernatant was transferred to 1.50 mL prelabeled and prechilled microcentrifuge tubes. Exactly 10.0 µL of each supernatant was transferred to a 500 µL prelabeled, prechilled microcentrifuge tube for use in a BCA assay that would determine protein content. The remaining soluble muscle homogenate was stored at -80.0 ^{o}C until further analysis.

Bicinchoninic assay (BCA)

A BCA protein assay was performed to determine protein concentration (Figure 12). A stock solution of BSA was prepared by measuring 48 mg albumin (Abcam) on an electronic triple beam balance and mixing with 10.0 mL phosphate buffered saline (PBS). Ten standards were prepared to suit the following concentrations: 600 µg/mL, 300 µg/mL, 150 µg/mL, 75 µg/mL, 37.5 µg/mL, 18.75 µg/mL, 9.375 µg/mL, 4.6875 µg/mL, 2.34375 µg/mL, and a blank negative control of 0 µg/mL. Muscle homogenate was allowed to thaw on ice while the standards were prepared. All muscle tissue samples were then diluted 1:20 using 15 µL of sample and 285 µL of PBS. 12000 µL of 1:50 working reagent was made for the assay by combining 11764.7 µL reagent A with 235.3 µL reagent B. This volume would allow enough working reagent for duplicates of the standards and unknown samples in a 96-well plate. 100 µL of standards and unknown samples were added to a 96-well clear bottom microplate, followed by 100 µL of working reagent. The plate was then sealed and incubated at 37.0 ^{o}C for 1 hour.

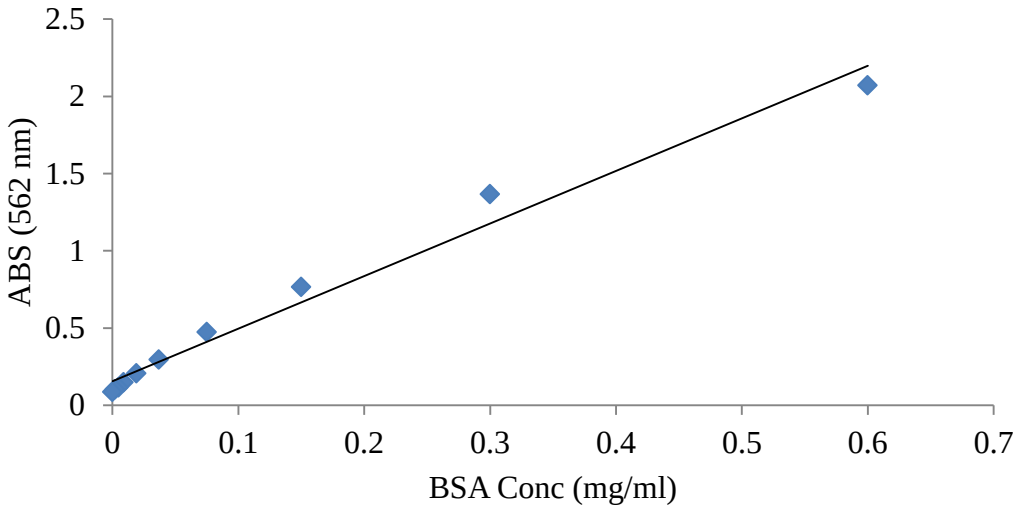

Figure 12: Standard curve for BCA protein assay of soleus muscle tissue. All unknown samples had absorbencies within this standard curve that allowed for interpolation and subsequent determination of protein concentration, followed by multiplying by a dilution factor of 20. Recording absorbance at 562 nm yielded a best-fit standard curve of $y = 3.4009x + 0.1564$, with $R^2 = 0.9799$.

The assay was performed using a Molecular Devices SpectraMax Paradigm machine. Paradigm SMP was opened and connected to the machine via computer. ABS-MONO was selected to begin the assay and the wavelength was set to 562 nm. The plate selected for the assay was defined as 96 Well Standard clrbtm. The reading area was highlighted and assignments were made to all standards and unknown samples. The plate was shaken on medium intensity for 5 seconds prior to reading absorbencies.

A standard curve was prepared by plotting the average absorbance of the standards against the designated concentration. The concentration of unknown samples was calculated using the standard curve best-fit equation and multiplying by the dilution factor of 20. Once the concentration of each sample was determined, total protein content could be determined for appropriate future Magpix analysis.

Absorbency data from Paradigm SMP were plotted and graphed in Excel to produce the standard curve. This curve was used for interpolation of sample protein concentration.

Magpix

Insulin in plasma samples were analyzed for comparison between LCR basal, LCR insulin-stimulated, HCR basal, and HCR insulin-stimulated groups at respective times directly preceding tissue harvest (t=0 min. for basal groups and t=120 min. for insulin-stimulated groups). In addition, insulin-stimulated groups of LCR and HCR rats were analyzed at both t=0 min. and t=120 min. Analysis protocol was carried out using the Rat Metabolic Magnetic Bead Panel by Milliplex® MAP Kit (Merck, Cat. #RMHMAG-84K). Antibody-immobilized beads were sonicated for 30 seconds and then

vortexed for 10 seconds. 150.0 µL of antibody was transferred and diluted in a mixing bottle with 2.85 mL of bead diluent (LE-BD). Quality controls 1 and 2 (RMH-6084) were reconstituted by adding 250.0 µL deionized water to each vial. These were vortexed and allowed to sit for 10 minutes before loading into a 96-well plate. Wash buffer (L-WB) was prepared by diluting 30.0 mL 10X wash buffer with 270.0 mL deionized water. 1.0 mL deionized water was added to reconstitute serum matrix (LRGT-SM) and this was allowed to sit 10.0 minutes prior to loading. Standards were prepared by reconstituting the metabolic standard (RMH-8084) with 250.0 µL deionized water and vortexing for 10 seconds. The vial was left to sit 10.0 minutes before performing serial dilutions to prepare a standard curve for the assay.

Two hundred microliters of assay buffer (LE-ABGLP) was added to each well of a 96-well plate and shaken for 10 minutes at room temperature before decanting the buffer solution and adding 25.0 µL of serum matrix to each well. 25.0 µL assay buffer was then added to each well in addition to 25.0 µL of standards, controls, or unknown plasma samples. 25.0 µL of magnetic beads were added to each well before the plate was sealed, covered in aluminum foil, and incubated on a shaker at 4.0 ^{o}C for 18 hours.

All reagents were allowed to come to room temperature before well contents were decanted. The plate was washed three times by first allowing the plate to rest upon a magnetic block for 60.0 seconds. Well contents were decanted, then the plate was washed with 200.0 µL wash buffer and shaken for 30 seconds at room temperature. After that, the plate was reattached to the magnet and allowed to sit for 60.0 seconds before again decanting. Immediately following the washing steps, 50.0 µL detection antibodies (RMH-1084) were added to each well. The plate was covered and shaken at room

temperature for 30.0 minutes. Then, without decanting, 50.0 µL Streptavidin-Phycoerythrin ((L-SAPE12) was added to each well and the plate was again covered and shaken for 30.0 minutes at room temperature. The 96-well plate was then washed three times in the same way mentioned previously. Finally, 100.0 µL wash buffer was added to resuspend the beads before the plate was read using Luminex xPONENT (Merck) software. Data from Luminex xPONENT were analyzed as mean fluorescence intensity and were saved in Excel files for analysis.

Total Akt and pAKT levels in each sample of muscle homogenate were also measured. A 2-plex total/phosphor Akt Magnetic Bead Kit (Cat. #48-618MAG) was used to analyze Akt content. To begin, reagents were prepared for the immunoassay per protocol guidelines. The 20x stock magnetic bead solution was sonicated for 15.0 seconds and then vortexed for 30.0 seconds. The beads (42-618MAG) were diluted to 1x concentration by transferring 150.0 µL stock solution into a mixing bottle with 2.85 mL assay buffer 2 (43-041). The biotin-labeled antibody was prepared by vortexing a 20x stock solution (44-618MAG) for 10.0 seconds and diluting 150.0 µL in a mixing bottle with 2.85 mL assay buffer 2. Streptavidin-Phycoerythrin (45-001H) was vortexed for 10.0 seconds and diluted by combining 120.0 µL in a mixing bottle with 2.88 mL assay buffer 2. Control cell lysates (47-205 and 47-216) were each reconstituted with 100.0 µL Millipore® water before being vortexed gently and incubated for 5.0 min at room temperature. 150.0 µL assay buffer 2 was then added to each cell lysate vial and the vials were vortexed gently before use in the assay.

All sample homogenate muscle concentrations were calculated using the standard curve. The samples were first allowed to thaw on ice before being diluted to 1.6 µg/µL

with working lysis buffer. Muscle samples were stored on ice per protocol recommendation. These samples were further diluted 1:1 with assay buffer 2 as suggested in the protocol, giving a final concentration of 20 µg in a 25 µL aliquot (20 µg / 25 µL after a 1:1 dilution with assay buffer 2).

Fifty microliters of assay buffer 2 was added to each well of a clean 96-well plate. The plate was covered and shaken at room temperature for 10.0 minutes. Assay buffer was decanted and 25.0 µL of the vortexed 1x bead suspension was added to each well. Following bead addition, 25.0 µL assay buffer, controls, and muscle homogenate samples were added to appropriate wells. The plate was sealed, covered in aluminum foil, and shaken at 4.0 ^{o}C for 20 hours.

Following cold incubation, the plate was washed with assay buffer two times as described previously. 25.0 µL of 1x detection antibody was added to each well and the plate was shaken at room temperature for 1 hour. The plate was attached to a magnetic block for 60.0 seconds and the antibody was decanted before the addition of 25.0 µL Streptavidin-Phycoerythrin to each well. The plate was again sealed and shaken for 15.0 min at room temperature. Without decanting the Streptavidin-Phycoerythrin, 25.0 µL amplification buffer (43-024A) was added. The plate was sealed again and shaken for 15.0 min at room temperature. Finally, the plate was attached to a magnetic block for 60.0 seconds before decanting the Streptavidin-Phycoerythrin and amplification buffer. Beads were resuspended with the addition of 150.0 µL assay buffer 2 in each well. The plate was shaken for 5.0 minutes at room temperature before reading the plate with Luminex xPONENT software.

Data from Luminex xPONENT were saved as mean fluorescence intensity and stored in an Excel file.

Statistical Analysis

Significance was initially set at $\alpha=0.05$. Two-tailed student's t-tests were performed on sample sizes greater than $n=13$ to compare body masses, food consumption, and rate of body mass increase. For *in vivo* data with small sample sizes, means were compared using Cohen's *d* with 95% confidence intervals. As mentioned previously, findings that appeared significant were further supported with two-tailed student's t-tests or wilcoxen-rank-sum to obtain p-values. Data are represented as mean +/- SEM.

RESULTS

Body Weight Gain and Food Consumption

Matching the rats based on body mass was a good way to exclude extraneous variables in the research design. Weight-matching the rats into separate groups yielded a negligible difference in mass at week 12 as well as at the time of tissue harvesting (Appendix A). Body weights were recorded weekly during a 12-week observational period, with LCR rats observed to have significantly higher body mass each week as compared to HCR rats, $p<0.001$ (Figure 13A).

Ad-libitum food consumption was observed to be constant over 12-week observation for both LCR and HCR groups (Figure 13B). LCR and HCR absolute food consumption data appear to overlap each week, showing no difference in consumption ($p=0.86$). Over the 12-week observational period, LCR and HCR rat groups gained appreciable mass (Figure 13A); however, HCR rats appeared to consume more food relative to body mass than LCR rats (Figure 14). Further supporting this observation, the rate at which mass was gained (Figure 15) was greater in LCR rats as compared to HCR rats ($p<0.05$). These data begin to suggest that intrinsic aerobic capacity may be responsible for the observed differences in basal metabolic rate (also see Appendix B). Together, these data may indicate a few things: HCR rats may have an increase in cage activity as compared to LCR rats, HCR rats may have heightened metabolic rate as compared to LCR rats, or the observed difference in basal metabolic rate between LCR and HCR rats may result from a combination of these suggestions.

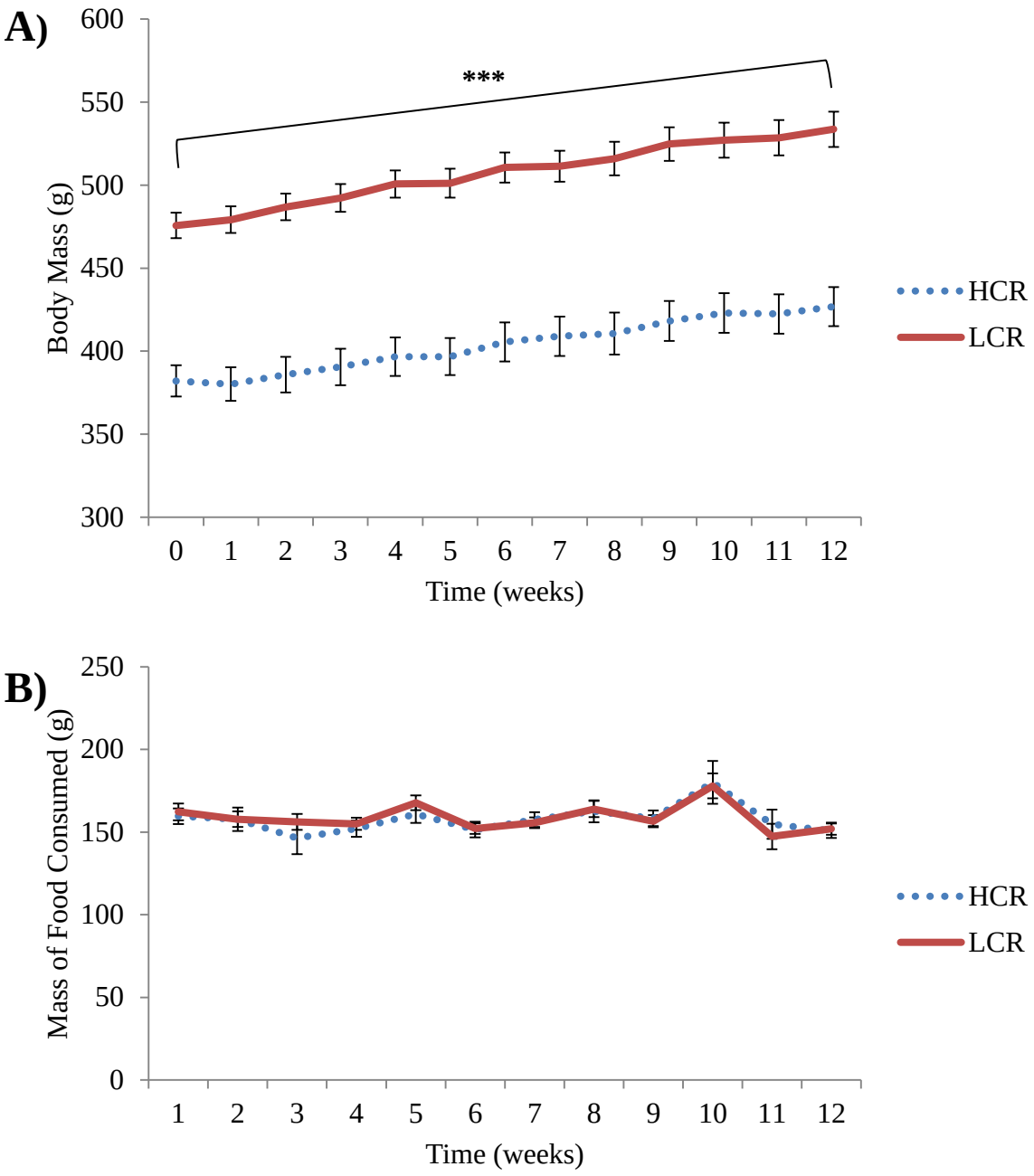

Figure 13: Body mass and food consumption during 12-week observation. **A)** Aerobic capacity influences body mass. LCR rats exhibited higher body masses than HCR rats during each week throughout the 12-week observation. Standard error bars are displayed for each week, with no overlap seen between groups. Both LCR and HCR rats appeared to have a positive rate of change in body mass. **B)** Food consumption did not differ between low and high aerobic capacity rat cohorts. Consumption appeared to be constant throughout 12-week observation with standard error bars shown to be overlapping ($p=0.86$), ***$p<0.001$.

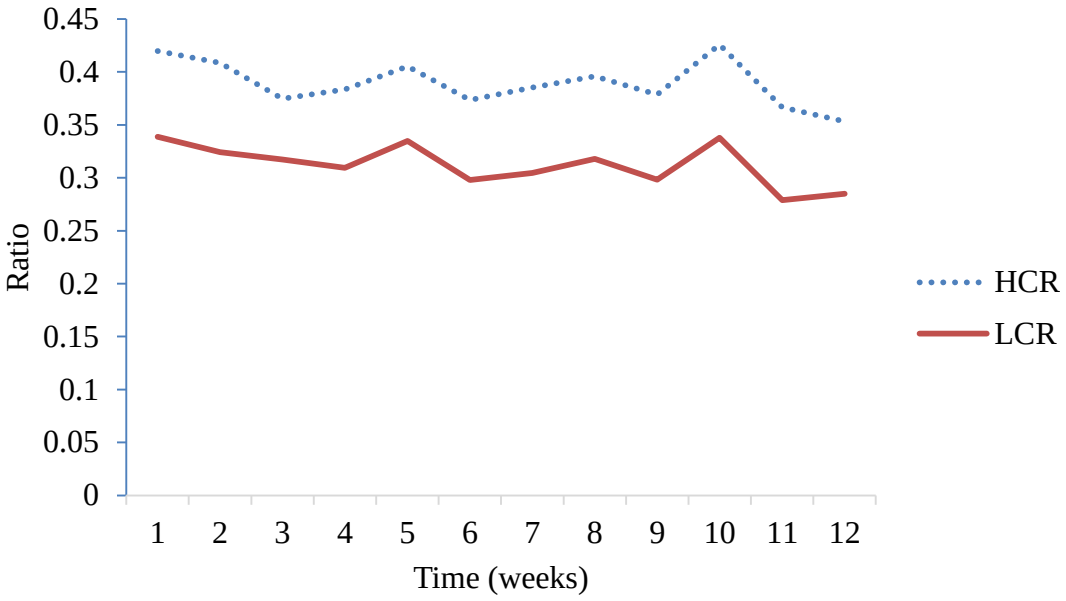

Figure 14**:** Food consumption of rat cohorts relative to body weight during 12-week observation. These data were transformed from figure 13, shown above. HCR rats appeared to consume more food relative to body weight than LCR rats, consistent throughout the entirety of observation.

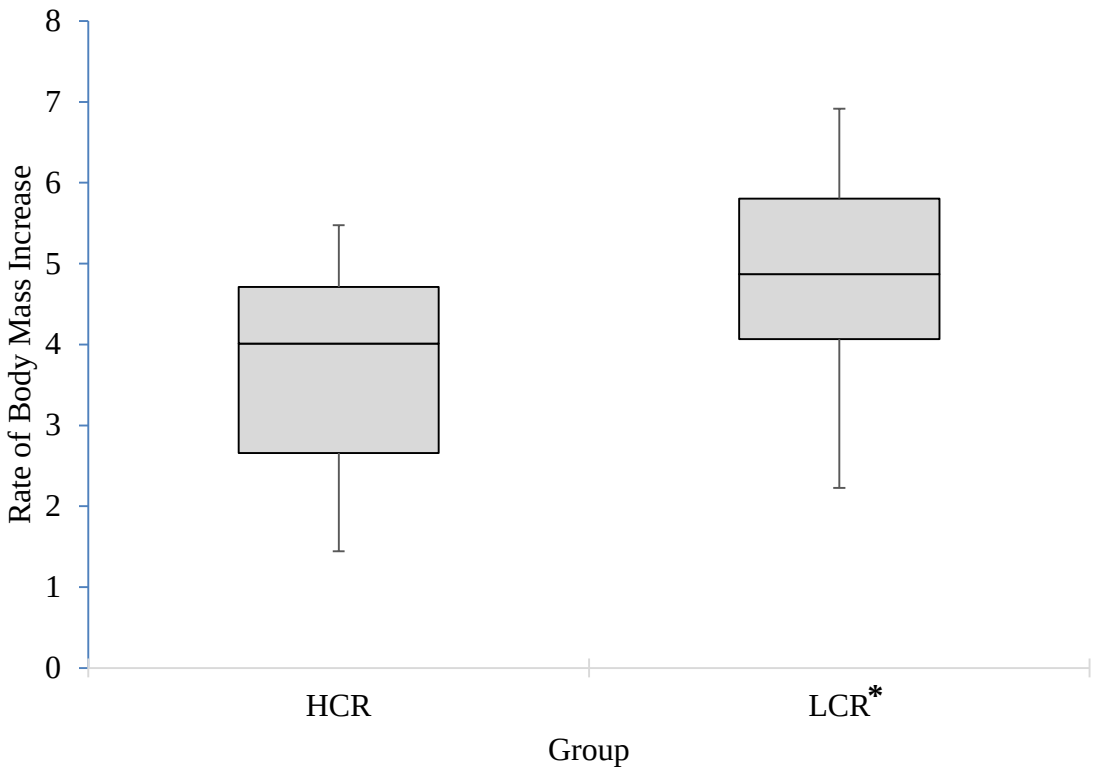

Figure 15: Side-by-side boxplots compare the rate of body mass change in low and high aerobic capacity rat models. Rate was calculated as total mass gained over time (g/week). It appeared there is a higher median rate of change in the LCR group (n=14) as compared with the HCR group (n=14). In addition, there appeared to be a slight positive skew in the HCR data as the median line is closer to the 75th percentile than to the 25th percentile. However, there did not appear to be any outliers in this dataset. The distribution of LCR appeared normal and without any outliers. The mean of each dataset were significantly different, *$p<0.05$.

Insulin Sensitivity is Reduced in LCR Rats During a Euglycemic-Hyperinsulinemic Clamp

A euglycemic-hyperinsulinemic clamp was performed as previously described above. After a 5-hour fast, baseline blood glucose readings did not differ between LCR and HCR rats at t=-10 min and t=0 min (p=0.47 and p=0.32, respectively). At t=0 min. hematocrit readings were taken and compared to levels taken at t=120 min. to ensure similar and minimal blood loss during the clamp procedure. Reliable and effective clamp data will have minimal blood loss and no difference in blood loss between groups. This study observed on average a 13% decrease in hematocrit levels for LCR and HCR rats, with no significant difference in hematocrit decrease between LCR and HCR rats following the clamp (p=0.45, data not shown). A metabolic clamp proceeds over 120 minutes with literature data suggesting a successful clamped value of blood glucose around 130 mg/dL, determined by the average value of the final few readings (Ayala et al. 2006). This supports a clamped value as being the average of values obtained between t=90 min. and t=120 min. Figure 16 shows the progression of blood glucose readings in LCR and HCR rats throughout the duration of the metabolic clamp procedure. There was no difference observed between LCR and HCR rat blood glucose levels between t=90 min. and t=120 min. (p=0.86, Figure 16A). LCR rats were observed to have an average clamped value of 130.5 mg/dL whereas HCR rats had an average clamped value of 134.2 mg/dL. These data yielded a Cohen's *d* value of 0.1324 (-1.31, 1.56) which further suggest there was no difference in clamped blood glucose levels during LCR and HCR metabolic clamp procedures, as standard error bars overlap (Figure 16B).

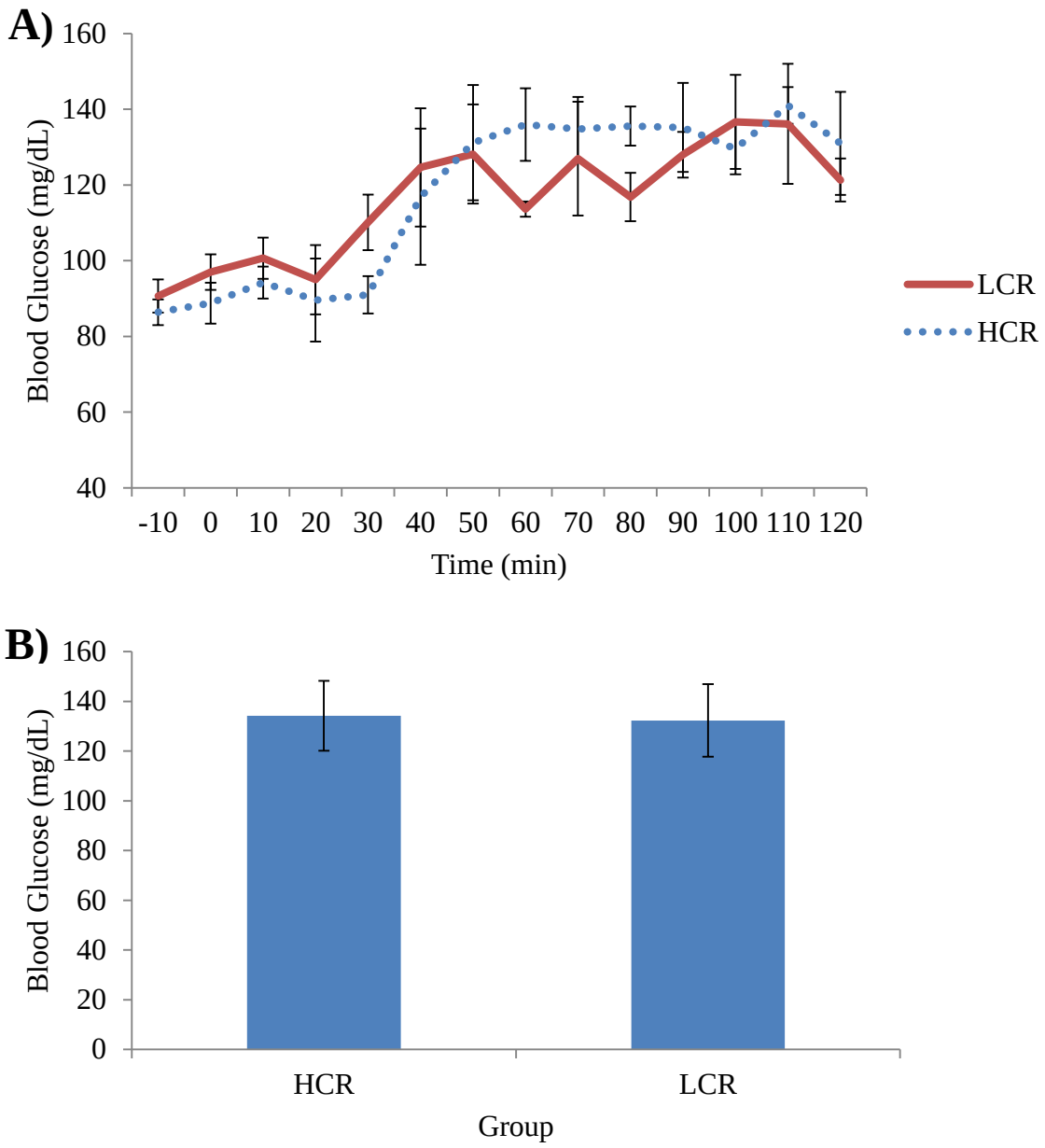

Figure 16: Blood glucose levels during metabolic clamp. Panel **A)** shows blood glucose levels during the metabolic clamp procedure. LCR (*n*=3) and HCR (*n*=5) rats had similar fasting glucose levels at t=-10 min. Blood glucose levels appear to follow a similar pattern as time progresses, eventually toward a targeted blood glucose reading of about 130 mg/dL. Literature data suggest clamped values of blood glucose occur between t=90 min. and t=120 min. During this time interval, no difference was observed between blood glucose readings for LCR and HCR rats as standard error bars overlap. Panel **B)** displays the mean (+/- standard error) clamped values for both LCR and HCR rats. Standard error bars overlap, suggesting there is no difference in values. When further comparing effect sizes, a Cohen's *d* value of 0.1324 was obtained with a 95% confidence interval of (-1.31, 1.56).

Glucose infusion rate was measured during the clamp procedure while rats were administered a constant infusion of insulin at 4 mU/kg/min. At t=30 min. there appears to start a difference in glucose infusion rate to maintain the clamped value of blood glucose concentration of 130 mg/dL (Figure 17A). Similar to the graph for blood glucose levels a clamped value of glucose infusion rate will be the average of the values recorded coinciding with the values used to determine the clamped value of blood glucose. In this study, the final 4 values of glucose infusion rate from t=90 min. through t=120 min. were used to determine a clamped value of glucose infusion. Figure 17A displays the progression of glucose infusion measurements throughout the duration of the metabolic clamp procedure. LCR rats were observed to have a clamped glucose infusion rate of 24.25 μg/g/min and HCR rats were observed to require an increased glucose infusion rate of 31.35 μg/g/min ($p<0.05$). A Cohen's *d* value of 1.856 (0.047, 3.569) was obtained for glucose infusion rate data, with no observed overlap in standard error bars (Figure 17B). Together, these data suggest that low intrinsic aerobic capacity causes insulin resistance.

Low Aerobic Capacity Reduces Soleus Muscle Mass, But Not Total Akt Content

There was no significant difference observed between soleus muscle mass in LCR and HCR rats ($p=0.624$). Error bars overlap with a 95% confidence interval of (-15.0, 28.5), further supporting the observation that there was no difference in soleus muscle mass (Figure 18A). Relative to body mass, HCR rats were observed to have increased soleus muscle mass when compared to LCR rats ($p<0.001$). The ratio of soleus muscle mass to total body mass appeared to be increased 1.5-fold in HCR rats as compared to

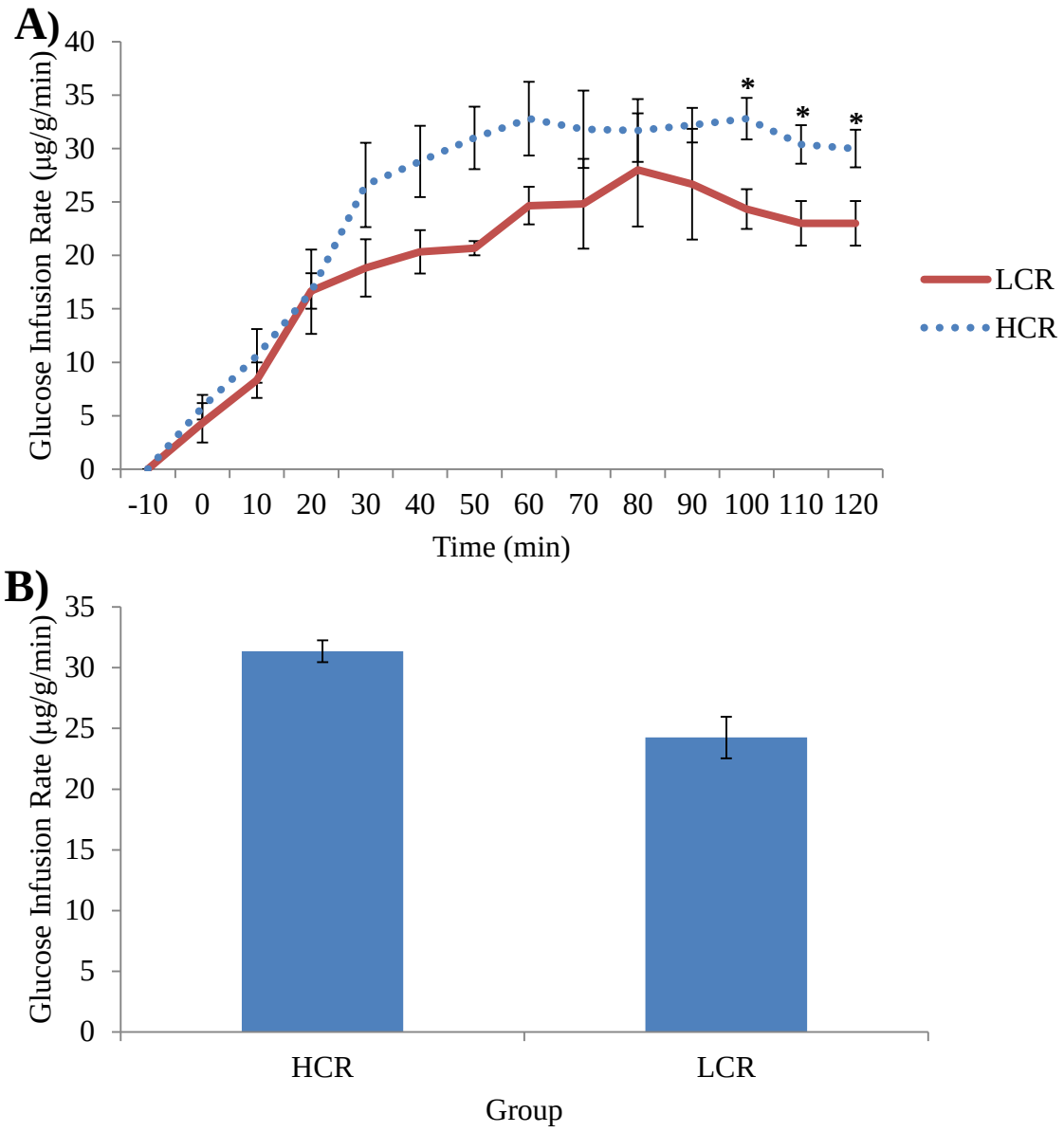

Figure 17: Glucose infusion rates during metabolic clamp. Panel **A)** displays the effect of aerobic capacity on glucose infusion rate. LCR (*n*=3) rats appeared to require lower rates of glucose infusion to maintain euglycemia during a clamp procedure than HCR (*n*=5) rats. Literature data suggest glucose infusion rate to be defined by the values recorded from t=90 min. through t=120 min. The data support a difference in average glucose infusion rate during these observations. Standard error bars are displayed for all time points with no observed overlap during t=100 min, t=110 min, nor t=120 min, which suggests a significant difference in glucose infusion rates. Panel **B)** displays the mean glucose infusion rate (+/- standard error) for LCR and HCR rats during the defined time points of t=90 min. through t=120 min. Standard error bars are displayed with no overlap, suggesting a significant difference between the two populations. Upon further comparison using effect sizes, a Cohen's *d* value of 1.856 was obtained with a 95% confidence interval of (0.047, 3.569), *p<0.05.

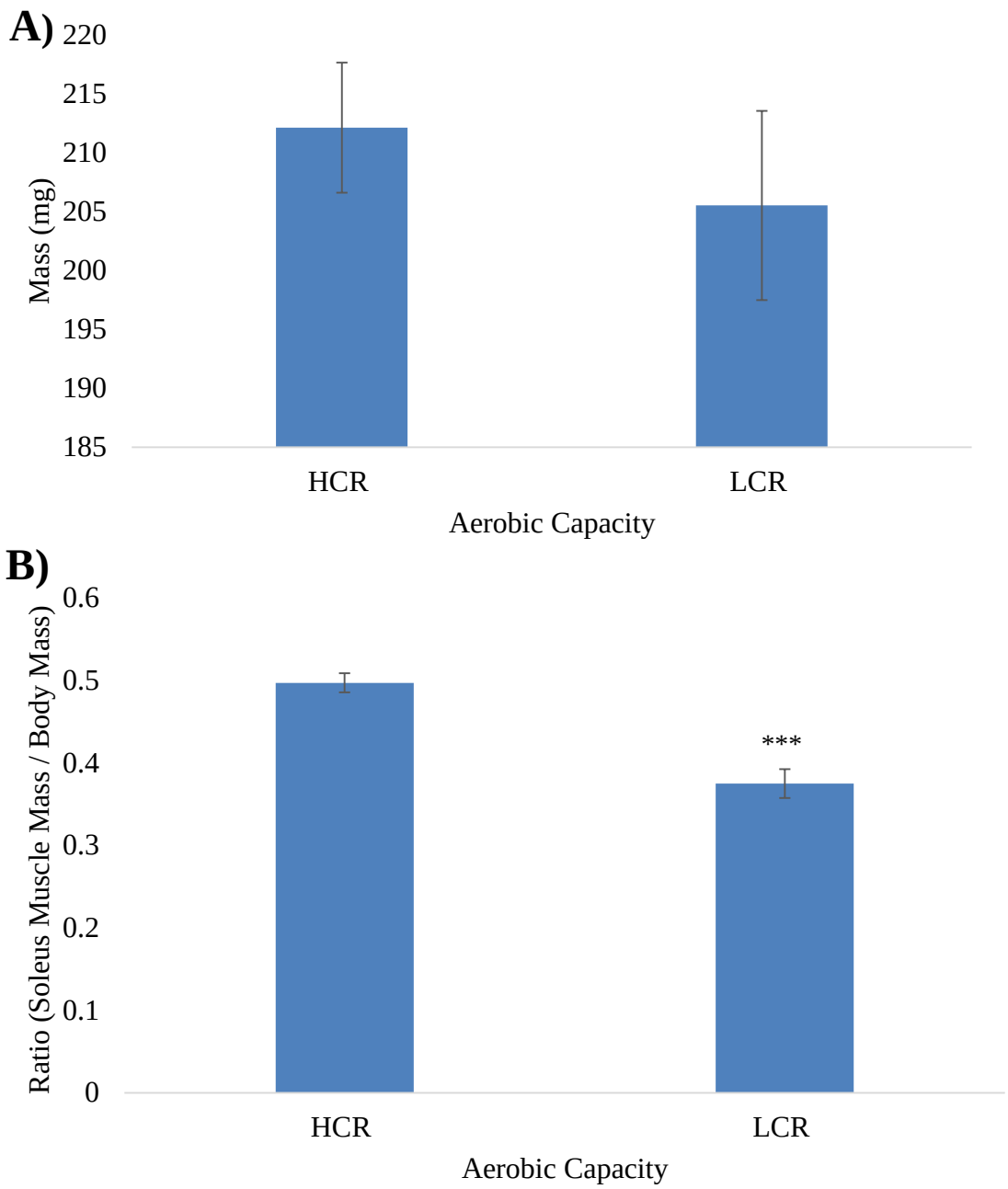

Figure 18: Aerobic capacity does not appear to directly influence soleus muscle mass, but may influence overall lean body mass. **A)** LCR rats (*n*=7) did not appear to have a significant difference in soleus muscle mass as compared to HCR rats (*n*=12). A p-value of 0.624 was obtained with 95% confidence interval of (-15.0, 28.5), which further suggests that aerobic capacity does not influence soleus muscle mass. **B)** Relative to overall body mass, HCR rats (*n*=12) exhibited a significantly greater proportion of soleus muscle mass as compared with LCR rats (*n*=7) which might suggest a role of intrinsic aerobic capacity in lean body mass, ***p<0.001.

LCR rats (Figure 18B). These data may suggest that high intrinsic aerobic capacity is associated with locomotor muscles as compared to low intrinsic aerobic capacity.

As a measure of skeletal muscle insulin signaling, total Akt content was determined in both LCR and HCR rats (Figure 19). These data suggested no difference in total soleus muscle Akt content between LCR and HCR rats ($p=0.482$). A Cohen's *d* value of 0.378 (-0.568, 1.313) was obtained to further support the observation. Collectively these results indicate that while aerobic capacity might not influence total Akt in comparable samples, aerobic capacity is associated with the size of the soleus muscle.

Aerobic Capacity and Skeletal Muscle Akt(Ser^{473}) Phosphorylation Following Insulin Stimulation

Plasma insulin concentrations were recorded in all groups immediately prior to tissue harvest. Aerobic capacity had no effect on LCR- and HCR-basal group insulin concentration (Figure 20A). Upon insulin stimulation, an increase in plasma insulin concentration was observed in HCR rats as expected ($p<0.05$). It appeared that LCR rats also had an increase in plasma insulin concentration upon insulin stimulation. For LCR rats, a Cohen's *d* value of 2.174 (0.130, 2.174) was obtained. Since the 95% confidence interval does not include 0, these data suggest a significant increase in plasma insulin levels as a result of insulin stimulation. These data did not yield a p-value of less than 0.05 only because variances were not assumed to be equal, it should be noted that the error bars do not overlap and that Cohen's *d* confidence interval supports a difference. Taken together, these data support a difference in insulin concentration between basal

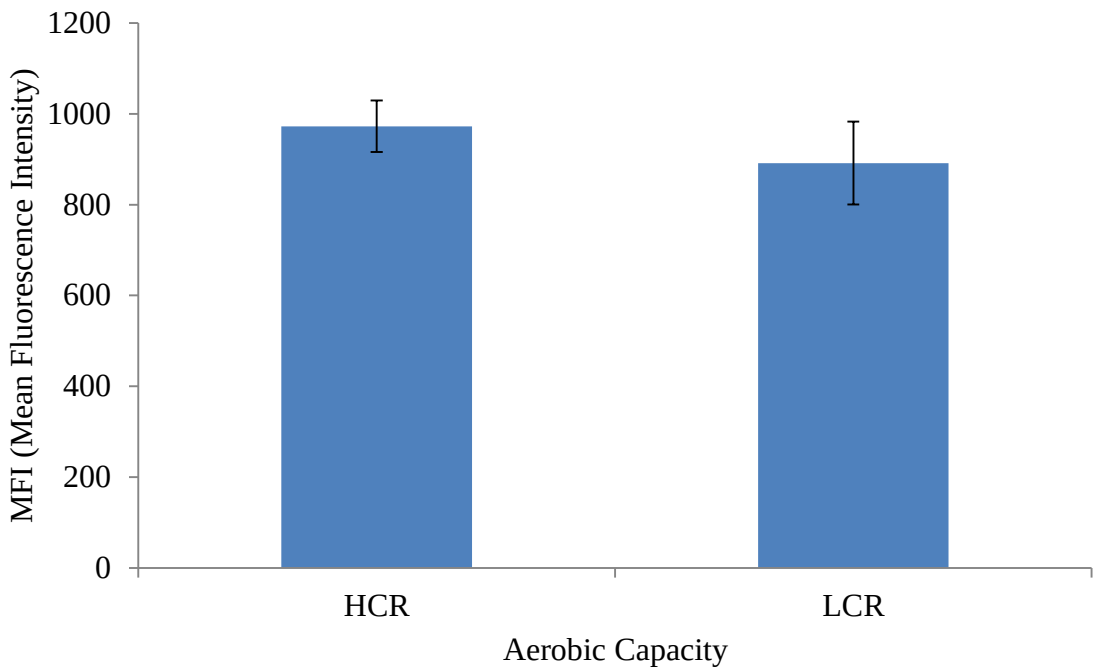

Figure 19: Aerobic capacity does not appear to influence total Akt content within skeletal muscle tissue. Data are presented as the mean value +/- standard error. There was no significant difference observed in the total amount of Akt within soleus muscle tissue of LCR rats (*n*=7) and HCR rats (*n*=12). Statistical analysis yielded a Cohen's *d* value of 0.378 with a 95% confidence interval of (-0.568, 1.313). Error bars overlap with p=0.482 and a 95% confidence interval of the difference in means being (-186.0, 336.63).

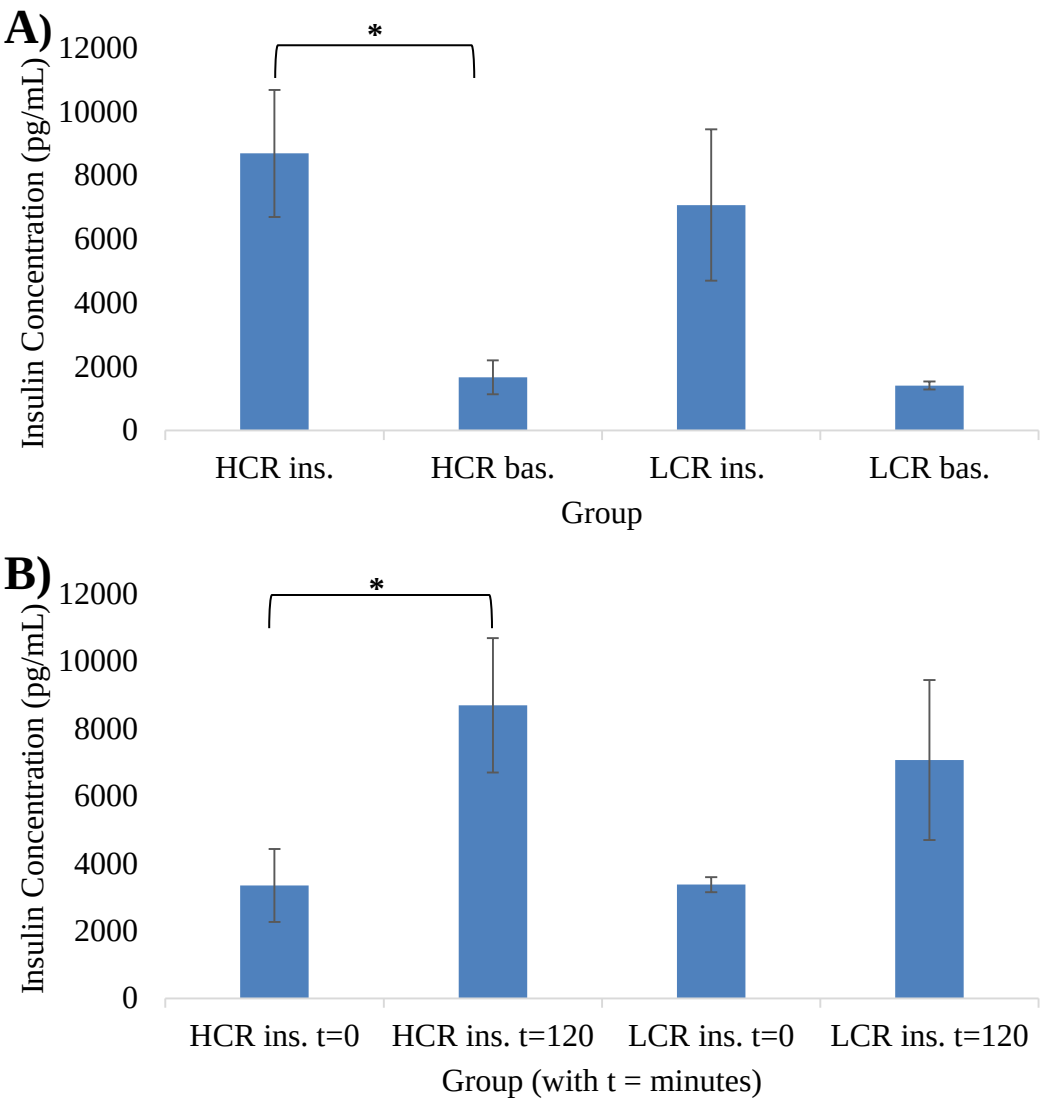

Figure 20: Plasma insulin concentration at time of tissue harvest and during the metabolic clamp procedure. **A)** There appears to be a 4-fold increase in plasma insulin concentration between HCR basal (*n*=7) and HCR insulin (*n*=5) groups. Statistical analysis of effect sizes gives Cohen's *d* value of -2.3268 (-3.821, -0.769). An apparent 5-fold increase in plasma insulin concentration between LCR basal (*n*=4) and LCR insulin (*n*=3) yielded Cohen's *d* value of 2.174 (0.130, 2.174). There was no observed difference between basal groups of LCR and HCR as Cohen's *d* = 0.224 (-1.015, 1.451). Similarly, no difference was observed between insulin-stimulated groups of LCR and HCR as Cohen's *d* = -0.373 (-1.804, 1.088). **B)** Plasma insulin concentration increased during the metabolic clamp procedure, yielding about a 3-fold increase in HCR rats [Cohen's *d* = -1.065 (-2.379, 0.304)] and a 2.5-fold increase in LCR rats [Cohen's *d* = -1.268 (-3.021, 0.601)] between t=0 min. and t=120 min. There did not appear to be a difference between HCR and LCR plasma insulin concentration neither at t=0 min. (-1.707, 1.172) nor t=120 min. (-1.399, 1.464) which suggests similar clearance in plasma insulin, *p<0.05.

and insulin-stimulated groups while negating any difference in insulin administration between LCR and HCR rats.

During the euglycemic-hyperinsulinemic clamp, HCR rats were observed to have an increase in plasma insulin concentration at t=120 min. when compared with t=0 min. ($p<0.05$, Figure 20B). Data suggest a 3-fold increase in plasma insulin concentration upon insulin administration throughout the clamp procedure. LCR rats appear likely to have observed an increase in plasma insulin at t=120 min. as compared with t=0 min. with a Cohen's *d* value of -1.268 (-3.021, 0.601). The interval suggests a lack of significance, probably due to variance and small sample size; however, error bars do not overlap and there still appears to be a 2.5-fold increase in plasma concentration. Further, there was no difference between LCR and HCR insulin levels at either t=0 min. (-1.707, 1.172) nor at t=120 min. (-1.1399, 1.464). Together, these data support a successful clamp procedure and suggest similar insulin clearance in both LCR and HCR rats.

Insulin will cause phosphorylation of Akt at Thr^{308} and Ser^{473} before facilitating GLUT4 translocation to the membrane for glucose uptake. Insulin-stimulated HCR rats were observed to have an increase in pAkt as compared to basal HCR rats ($p<0.05$, Figure 21). This supports the expected observation upon insulin-stimulation.

Insulin-stimulated LCR rats were observed to have a similar fold-change in pAkt levels as HCR counterparts, but the increase was not statistically significant. A Cohen's *d* value for basal and insulin-stimulated LCR rats was calculated to be -1.1045 (-2.698, 0.578). Error bars appear to overlap even though mean values mimic HCR data. No difference was observed between HCR basal and LCR basal groups (-1.486, 1.159); no

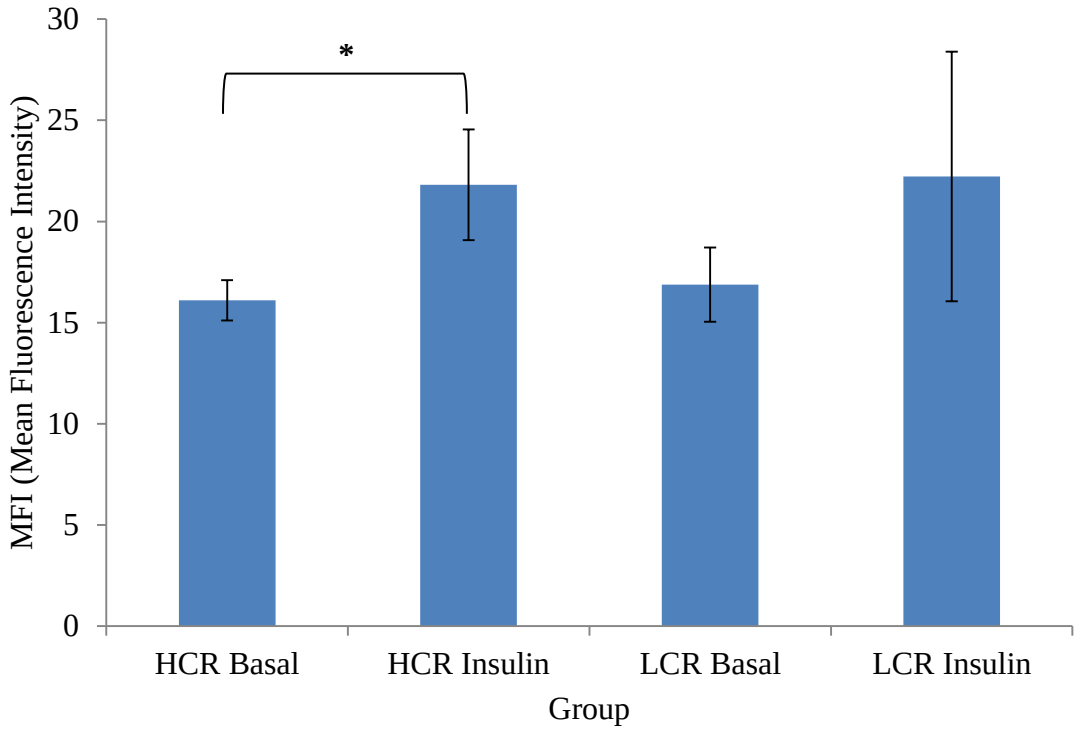

Figure 21: Basal and insulin-stimulated pAkt in rats of low and high aerobic capacity. Data are shown as mean values +/- standard error. Upon insulin administration, there appears to be an increase in phospho-Akt (Ser^{473}) between HCR basal (*n*=7) and HCR insulin-stimulated (*n*=5) groups. Statistical support is indicated with a Cohen's *d* value of -1.306 and a 95% confidence interval of (-2.559, -0.001). In addition, an increase in phospho-Akt (Ser473) might exist between LCR basal (*n*=4) and LCR insulin-stimulated (*n*=3) groups with an observed Cohen's *d* value of -1.1045 and 95% confidence interval (-2.698, 0.578). There was no statistical difference between LCR basal and HCR basal groups as effect size analysis yielded a Cohen's *d* value of -0.2587 and a 95% confidence interval of (-1.486, 1.159). Further, there was no statistical difference between LCR insulin-stimulated and HCR insulin-stimulated groups as effect size analysis yielded a Cohen's *d* value of -0.0508 and a 95% confidence interval of (-1.48, 1.38) *p<0.05.

difference was observed between insulin-stimulated groups of LCR and HCR rats (-1.48, 1.38). This figure supports insulin as directly influencing Akt phosphorylation within soleus muscle tissue and begins to suggest that a difference in Akt phosphorylation might not depend on aerobic capacity in slow, oxidative muscle fibers.

When pAkt data were normalized to total Akt levels, insulin-stimulated HCR rats had a greater proportion of pAkt as compared to basal HCR rats ($p<0.05$, Figure 22). LCR rats observed similar fold-changes in data; however, the increase was not statistically significant. The figure shows elevated levels of phspho-Akt (Ser^{473}) relative to total Akt content in insulin-stimulated soleus muscle tissue of HCR rats (n=5) as compared to basal HCR rats (n=7). A Cohen's d value of -0.7184 (-2.244, 0.872) might suggest that a true difference exists in normalized pAkt values observed between basal LCR and insulin-stimulated LCR rats. Further, there was no difference observed in normalized pAkt values between basal groups of HCR and LCR rats (-0.722, 1.785). There did not appear to be any significant difference in levels of phospho-Akt (Ser^{473}) in insulin-stimulated soleus muscle tissue of LCR rats (n=3) as compared to basal LCR rats (n=4). No difference was observed between insulin-stimulated groups of HCR and LCR rats (-1.626, 1.246). Together, these data suggest that low aerobic capacity may hinder phosphorylation of Akt(Ser^{473}) in insulin signaling pathways.

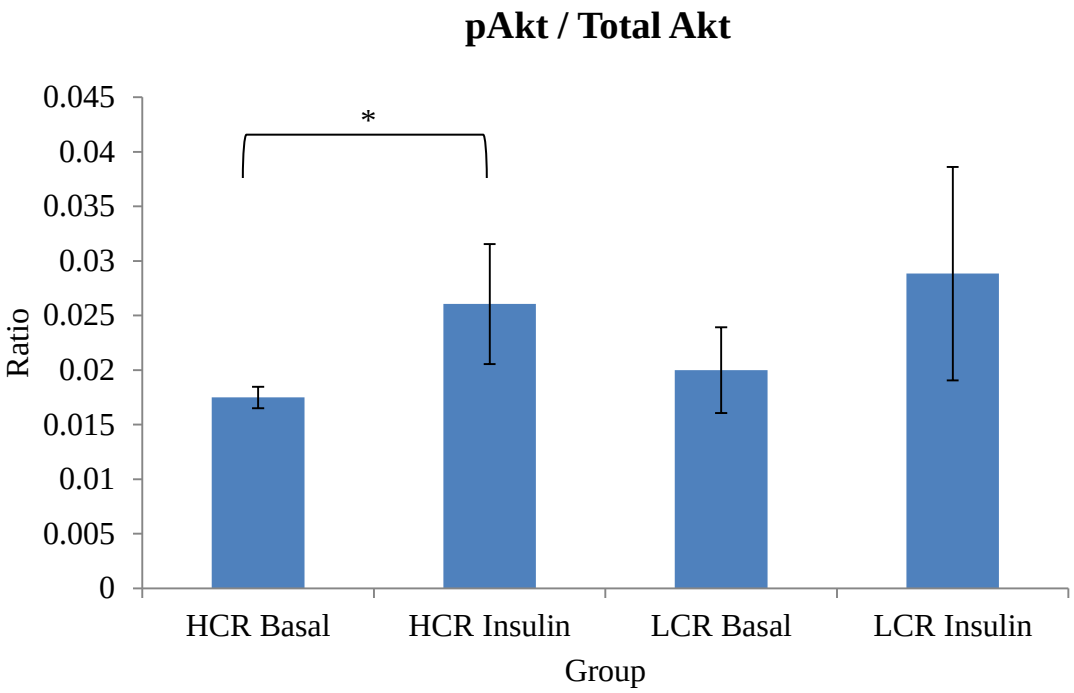

Figure 22: Ratio of phospho-Akt (Ser^{473}) to total Akt content within soleus muscle tissue. Data are presented as the mean value +/- standard error. No overlap of standard error occurs, and further analysis of effect sizes yielded a Cohen's *d* value of -1.0654 with 95% confidence interval (-2.279, 0.194). Statistical analysis using effect sizes showed a Cohen's *d* value of -0.7184 with 95% confidence interval (-2.244, 0.872). Further, there was no observed difference between HCR basal and LCR basal groups as effect size analysis gave Cohen's *d* value of 0.499 with 95% confidence interval (-0.722, 1.785). No difference was observed between insulin-stimulated muscle tissue in LCR and HCR rats as effect size analysis yielded Cohen's *d* value of -0.1982 with 95% confidence interval (-1.626, 1.246). *$p<0.05$

DISCUSSION

Aerobic capacity is associated with insulin signaling *in vitro*, but limited evidence has been demonstrated *in vivo* (Lessard et al. 2011; Medeiros et al. 2010). Recent data supports Akt phosphorylation at Ser^{473} to be a key, proximal insulin signaling event related to insulin resistance in humans (Friedrichsen et al. 2010). Therefore, an association may exist between Akt phosphorylation and *in vivo* insulin sensitivity. The present study examined the effect of aerobic capacity on insulin sensitivity and skeletal muscle insulin signaling in conscious, unrestrained rat models of low and high aerobic capacities. The focus of this research was to ascertain whether proximal insulin signaling mechanisms, such as Akt phosphorylation at Ser^{473}, are associated with systemic insulin resistance.

Several factors limit this study. These include the following: small sample size (n=3-5), mortality rate during surgical procedures, metabolic clamp complications, and sensitivity of signaling assays. Small sample sizes were largely due to mortality rate during surgery. It is interesting to note that HCR rats appeared to recover better from both catheterization and sham surgeries as compared to LCR rats (data not shown). During the clamp procedure, tubes disconnected the infusion pumps to catheters for a brief period of time during two IS metabolic clamps, but these were immediately reattached and measurements resumed. The euglycemic-hyperinsulinemic clamp procedure was effective in determining insulin sensitivity of rats completing the clamp proecedure (n=3-5). However, one LCR-IS rat was excluded from the study because of complications

during this metabolic clamp procedure. These complications included blood loss from the arterial line and difficulty maintaining constant infusions of insulin and glucose.

Another source of error may have been a result of establishing the phospho-Akt/total Akt signaling assay in the Morris Lab. Trial runs with select samples did not initially produce expected fold-changes in phospho-Akt(Ser^{473}) for positive controls. A new Akt signaling assay was used to troubleshoot the initial observations. The new kit produced a 1- or 2-fold increase in Akt phosphorylation (Ser^{473}) from baseline to insulin-stimulated samples. All remaining samples were then analyzed following this verification step.

The results obtained support an association between low aerobic capacity and a greater rate of physiological weight gain (Figures 13, 14, And 15). LCR and HCR rats in this study began acclimation at 20+/-2 weeks of age. Body mass measurements began at 22+/-2 weeks of age, with there already being a significant difference in mass between LCR and HCR rats. It is likely that HCR rats were more physically active within housing cages than LCR rats, thus contributing to differences observed in mass measurements. An increase in physical activity has been observed in HCR rats as compared to LCR rats following both normal chow and high-fat diets (Novak et al. 2010). Within skeletal muscle of LCR and HCR rats, an increase in physical activity was attributed to elevated levels of PEPCK-C in HCR rats as compared with LCR rats. This enzyme functions in gluconeogenesis and its overexpression is consistently linked with extended endurance and longevity (Novak et al. 2010). Thus, it is likely that this contributed to the lower observed body mass measurements in HCR rats.

Ad libitum food consumption was not different between groups (p=0.86), which suggests absolute caloric intake had no contribution to differences observed in body mass. Further, HCR rats consumed greater amounts of food relative to body mass each week as compared with LCR rats. HCR rats consistently weighed less with increased food consumption per gram of body weight throughout the duration of the study (Figure 14). These data may suggest a greater basal metabolic rate in HCR rats as compared to LCR rats. Furthermore, the rate of physiological body mass increase was significantly less in HCR rats than LCR rats (Figure 15). Together, these data support an inherent difference in physiological weight gained between LCR and HCR rats. Therefore, elevated energy expenditure due to physical activity and higher basal metabolic rates in HCR rats could be linked to improved energy homeostasis and decreased body weight as compared to LCR rats.

These data support previous observations suggesting the association between physical inactivity and obesity (Tremblay and Willms 2003). Exercise training has been associated with increases in working aerobic capacity over a defined time interval and metabolic enzymatic adaptations (Henriksson and Reitmann 1977). Together, these data begin to suggest physical inactivity might be associated with lower levels of working aerobic capacity, which can lead to increased weight gain and increased risk of obesity.

In addition, HCR rats had increased insulin sensitivity *in vivo* through use of a euglycemic-hyperinsulinemic clamp (Figure 17). This clamp procedure is a "gold-standard" when determining insulin sensitivity (Ayala et al. 2011). LCR rats were observed to be less insulin-sensitive as compared to HCR rats. The higher observed body weights in LCR rats as compared with HCR rats may contribute to these observations. As

mentioned before, the final four time values, t=90-120 min., were used when determining the mean value of glucose infusion rate (GIR). At t=30 min. GIR (mg/kg/min) began to diverge between LCR and HCR rats (Figure 17A). The lower GIR (mg/kg/min) observed in LCR rats is indicative of systemic insulin resistance. Together, these data show aerobic capacity influences GIR (mg/kg/min) in response to a constant infusion of insulin.

A reduction in GIR suggests LCR rats are more insulin resistant than HCR rats. The reduction in glucose uptake begins to mimic a TIIDM phenotype, which may support insulin resistance as a link between physical inactivity and diabetes (Campbell and Reece 2005). Previous studies consistently link physical activity with improved insulin sensitivity (Lessard et al. 2011; Medeiros et al. 2010; Hamilton et al. 2014). To determine which part of the insulin signaling pathway was responsible for the reduction in glucose uptake, soleus muscle tissues were analyzed for total and phosphorylated Akt content, since Akt phosphorylation is imperative for insulin-stimulated skeletal muscle glucose uptake (Gonzales and McGraw 2009; Stanford and Goodyear 2014; Figure 23).

Magpix protein assays helped determine the impact of aerobic capacity on skeletal muscle Akt phosphorylation *in vivo* (Figures 20, 21, and 22). Our hypothesis was that LCR rats would have impaired Akt phosphorylation that accompanies the observed decrease in GIR. HCR rats were observed to have an increase in Akt phosphorylation upon insulin-stimulation while LCR rats did not demonstrate the same significant increase in Akt phosphorylation when stimulated with insulin. Aerobic capacity does not appear to significantly influence the total amount of Akt present within the cell (Figure 20). However, intrinsic aerobic capacity appears to influence the consistency of phospho-Akt(Ser^{473}) and the ratio of phospho-Akt(Ser^{473}) / total Akt in HCR rats. Significant

increases in absolute and normalized Akt phosphorylation were not observed in LCR rats (Figures 21 and 22, respectively). Therefore, the observed increase in Akt phosphorylation in HCR rats is not simply due to an increased amount of Akt. Instead, these data begin to suggest a reduction in the consistency of Akt phosphorylation in LCR-IS rats.

Akt phosphorylation is known to increase upon insulin administration (Bruss et al. 2005). Given this observation, these data suggest that LCR rats may have impairments in Akt phosphorylation relative to HCR rats. Taken together, these data might be interpreted to suggest the difference in systemic insulin sensitivity observed between LCR and HCR rats is mediated through a difference in Akt signaling. Figures 21 and 22 show a significant increase in phospho-Akt(Ser^{473}) in HCR-IS rats, but not in LCR-IS rats. However, neither basal nor insulin-stimulated levels of phospho-Akt(Ser^{473}) were significantly different between LCR-IS and HCR-IS rats (Figures 21 and 22). These observations do imply a convincing argument for any impairment in insulin-stimulated Akt phosphorylation. Mean values of total Akt and pAkt did not differ between LCR-IS and HCR-IS rats, which may indicate intact insulin signaling at the level of Akt phosphorylation.

The lower value of GIR observed in LCR rats could be attributed to other mechanisms involved in glucose homeostasis. These may include elevated liver glucose production or impaired delivery of substrate to insulin-stimulated skeletal muscle. Together, these data do not provide a convincing argument to suggest low aerobic capacity is associated with impairments in Akt phosphorylation. Thus, the reduction in GIR observed in LCR rats might be attributed to a reduction in protein activation

downstream Akt. A good direction for future studies may be to focus on expression and activation of TBC1D1, AS160, and GLUT4 (Figure 23).

Small sample sizes likely contributed to high variability in Akt signaling. Standard error bars overlapped in data presentation of total Akt (Figures 21 and 22), and increasing sample sizes would reduce standard error. The 95% confidence interval around Cohen's *d* was (-0.568, 1.313), which includes 0 and is interpreted as not being significant. However, the upper end of this range may indicate a significant difference exists. Similarly, reducing the observed error in phospho-Akt(Ser^{473}) through an increase in sample size might strengthen the data (Figures 21 and 22).

Future studies include replicating results and increasing sample sizes. Impaired insulin-stimulated phosphorylation of Akt could lead to impairments in insulin-stimulated GLUT4 translocation to the membrane for glucose uptake. Other insulin-stimulated targets of interest include phosphorylation of AS160 or TBC1D1. These distal phosphorylation steps have been implicated in both insulin-stimulated and contraction-induced glucose uptake in muscle (Cartree et al. 2007, Taylor et al. 2008). If these data were replicated and absolute values of Akt phosphorylation did not differ between LCR and HCR rats, then the impairment in insulin-stimulated glucose uptake must occur distal to Akt phosphorylation. Skeletal muscle glucose uptake is influenced by insulin-stimulation as well as compensatory pathways influenced through exercise (Figure 23). Glucose uptake and exercise-mediated GLUT4 translocation is not impaired during acute bouts of exercise in mice lacking skeletal muscle insulin receptors (Stanford and Goodyear 2015). These findings may provide future avenues for understanding the

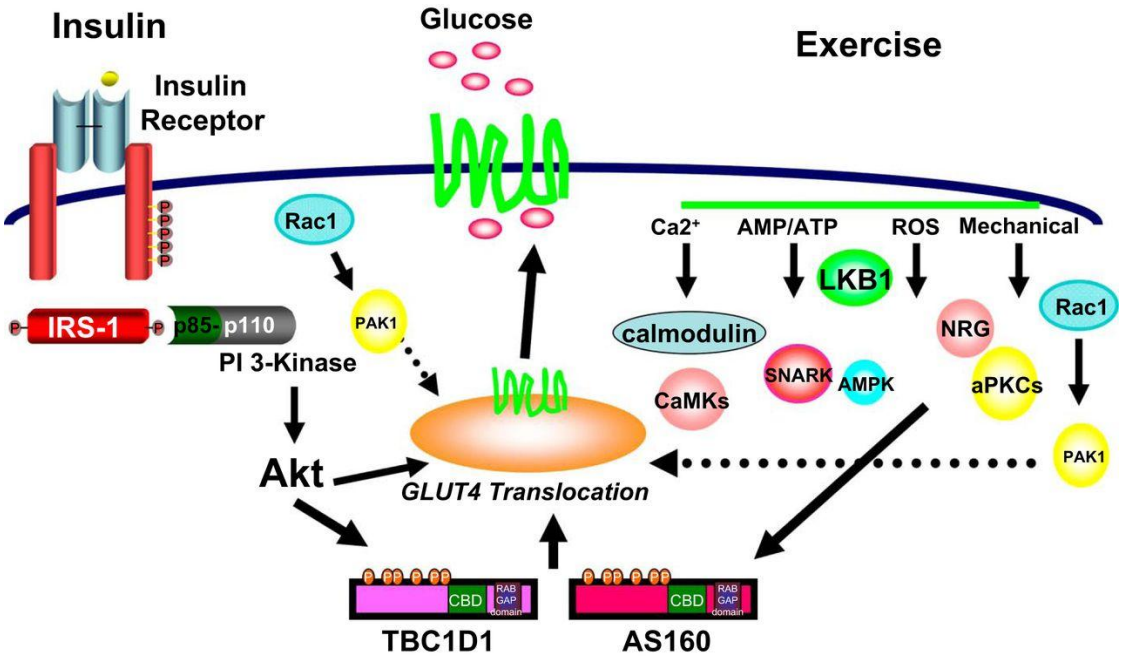

Figure 23: Exercise and insulin regulation of glucose transport (Stanford and Goodyear 2015). This figure highlights insulin signaling for glucose uptake and proposes several compensatory mechanisms for GLUT4 translocation upon an exercise-induced increase in skeletal muscle contraction.

mechanisms responsible for the observed LCR reduction in GIR as compared to HCR rats.

These results require further study to clarify the role of aerobic capacity in skeletal muscle insulin signaling during glucose uptake. Akt phosphorylation will be analyzed in vastus lateralis (type II fiber) and plantaris (type I and type II fibers) muscle tissues. If a difference in signaling activity is observed, a proteomic assay will be performed to assess phosphorylation activity of several metabolic proteins within the cell.

Consistent with previous studies, our data support LCR rats have higher rates of physiological weight gain compared to HCR rats. LCR rats also had lower GIR during a euglycemic-hyperinsulinemic clamp as compared to HCR rats. This clamp procedure has been performed previously in mice (Ayala et al. 2011) and has now been established in LCR and HCR rats. This rat model has become a powerful tool in exploring potential epigenetic mechanisms of metabolic abnormalities. Insulin signaling was measured using Akt as a marker for pathway activity. Akt was selected because it is known to become phosphorylated upon insulin-stimulation and provides just one of many indications of insulin responsiveness (Bruss et al. 2005). Total Akt and phospho-Akt (Ser^{473}) were measured using a multiplex ELISA that allowed for detection of both antibodies within a single sample. Therefore, the assay reduced error from multiple samples and gave a novel approach to protein detection within muscle samples. LCR-IS rats showed a reduction in fold-change expected from insulin-stimulation in both absolute and normalized phospho-Akt(Ser^{-473}) as compared to HCR-IS rats; however, the mean values of total Akt and phospho-Akt(Ser^{473}) were not different between LCR-IS and HCR-IS rats. This may

imply distal impairments in glucose uptake, including activation of AS160, TBC1D1, or total GLUT4 expresison.

To recapitulate, the mechanism(s) linking physical inactivity, diabetes, and obesity are still unclear; however, insulin resistance is observed in each phenomena and might be what links these three together. An unbiased, heterogeneous rat model was used to elucidate the impact of functional aerobic capacity on physiological weight gain, systemic insulin sensitivity, and insulin-stimulated glucose uptake. Rats of low and high aerobic capacities provided groups that mimic low and high levels of physical fitness. Data suggested low aerobic capacity, and therefore lower levels of physical fitness, were associated with increased physiological weight gain and reductions in insulin sensitivity as compared to high aerobic capacity, or those with higher levels of physical fitness. Together, these findings imply an association between physical inactivity, obesity, and diabetes through reductions in insulin sensitivity. However, insulin signaling data are yet inconclusive in determining where there is impairment in insulin-stimulated skeletal muscle glucose uptake (Figures 20, 21, and 22). Future studies may confirm insulin resistance at the level of Akt in other skeletal muscle fiber types (vastus lateralis type II, plantaris type I and II) or suggest distal impairments in insulin-stimulated glucose uptake.

In short, insulin resistance appears to be a linking mechanism between diabetes, physical inactivity, and obesity. We used a nonbiased rat model to assess the impact of aerobic capacity on insulin-stimulated glucose uptake and Akt activity. The results begin to suggest a difference in Akt activity between LCR and HCR rats; however, the data are not yet convincing to make a definite conclusion of insulin signaling impairment at that

level. Thus, future studies will either confirm impairment at Akt or suggest distal impairment in insulin-stimulated glucose uptake.

REFERENCES

Ayala JE, Bracy DP, Julien BM, Rottman JN, Fueger PT, Wasserman DH. 2007. Chronic treatment with sildenafil improves energy balance and insulin action in high fat-fed conscious mice. Diabetes. 56(4):1025-1033.

Ayala JE, Bracy DP, Malabanan C, James FD, Ansari T, Fueger PT, McGuinness OP, Wasserman DH. 2011. Hyperinsulinemic-euglycemic clamps in conscious, unrestrained mice. Journal of Visualized Experiments. 57:e3188.

Ayala JE, Bracy DP, McGuinness OP, Wasserman DH. 2006. Considerations in the design of hyperinsulinemic-eyglycemic clamps in the conscious mouse. Diabetes. 55(2):390-397.

Bamman MM, Cooper DM, Booth FW, Chin ER, Neufer PD, Trappe S, Lightfood JT, Kraus WE, Joyner MJ. 2014. Exercise biology and medicine: innovative research to improve global health. Mayo Clinic Proceedings. 89(2):148-153.

Biessels GJ and Kappelle LJ. 2005. Increased risk of Alzheimer's disease in Type II diabetes: insulin resistance of the brain or insulin-induced amyloid pathology? Biochemical Society Transactions. 33(5):1041-1044.

Bornfeldt KE and Tabas I. 2011. Insulin resistance, hyperglycemia, and atherosclerosis. Cell Metabolism. 14:575-585.

Bruce RA. 1984. Exercise, functional aerobic capacity, and aging—another viewpoint. Medicine and Science in Sports and Exercise. 16(1):8-13.

Bruss MD, Arias EB, Lienhard GE, Cartee GD. 2005. Increased phosphorylation of Akt substrate of 160 kDa (AS160) in rat skeletal muscle in response to insulin or contractile activity. Diabetes. 54(1):41-50.

Campbell NA and Reece JB. 2005. Biology. Seventh Edition. Pearson Education Inc. San Fransisco, CA. pp. 955-956.

Cartree GD and Wojtaszewski JFP. 2007. Role of Akt substrate of 160 kDa in insulin-stimulated and contraction-stimulated glucose transport. Applied Physiology, Nutrition, and Metabolism. 32(3):557-566.

Caspersen CJ, Powell KE, Christenson GM. 1985. Physical activity, exercise, and physical fitness: definitions and distinctions for health-related research. Public Health Reports. 100(2):126-131.

Cell Signaling Technology. 2010-2014. Insulin receptor signaling pathway. Accessed 21 April 2014 from http://www.cellsignal.com/contents/science-pathway-research-cellular-metabolism/insulin-receptor-signaling-pathway/pathways-irs.

Centers for Disease Control. 2009. Diabetes Public Health Resource: Diabetes Interactive Atlas. Accessed 21 April 2014 from http://www.cdc.gov/diabetes/atlas/countydata/atlas.html.

Centers for Disease Control. 2011. Physical Activity and Health: The Benefits of Physical Activity. Accessed 26 January 2015 from http://www.cdc.gov/physicalactivity/everyone/health/index.html.

Centers for Disease Control. 2014. Facts About Physical Activity. Accessed 26 January 2015 from http://www.cdc.gov/physicalactivity/data/facts.html.

Chang L, Chiang SH, Saltiel AR. 2004. Insulin signaling and the regulation of glucose transport. Molecular Medicine. 10(7-12):65-71.

Dash S, Sano H, Rochford JJ, Semple RK, Yeo G, Hyden CSS, Soos MA, Clark J, Rodin A, Langenberg C, Druet C, et al. 2009. A truncation mutation in *TBC1D4* in a family with acanthosis nigricans and postprandial hyperinsulinemia. Proceedings of the National Academy of Science. 106(23):9350-9355.

De Felice FG, Lourenco MV, Ferreira ST. 2014. How does brain insulin resistance develop in Alzheimer's disease? Alzheimer's & Dementia. 10:S26-S32.

Dwyer-Lindgren L, Freedman G, Engell RE, Fleming TD, Lim SS, Murray CJL, Mokdad AH. 2013. Prevalence of physical activity and obesity in US counties, 2001-2011: a road map for action. Population Health Metrics. 11:7.

Ferreira ST, Clarke JR, Bomfim TR, De Felice FG. 2014. Inflammation, defective insulin signaling, and neuronal dysfunction in Alzheimer's disease. Alzheimer's & Dementia. 10:S76-S83.

Friedrichsen M, Poulsen P, Richter EA, Hansen BF, Birk JB, Ribel-Madsen R, Stender-Petersen K, Nilsson E, Beck-Nielsen H, Vaag A, Wojtaszewski JFP. 2010. Differential aetiology and impact of phosphoinositide 3-kinase (PI3K) and Akt signaling in skeletal muscle on in vivo insulin action. Diabetologia. 53:1998-2007.

Gaesser GA and Rich RG. 1984. Effects of high- and low-intensity exercise training on aerobic capacity and blood lipids. Medicine and Science in Sports and Exercise. 16(3):269-274.

Gonzalez E and McGraw TE. 2009. The Akt kinases. Cell Cycle. 8(16):2502-2508.

Hamilton MT, Hamilton DG, Zderic TW. 2014. Sedentary behavior as a mediator of type 2 diabetes. Diabetes and Physical Activity. 60:11-26.

Hartree W and Hill AV. 1923. The anaerobic processes involved in muscular activity. The Journal of Physiology. 58(2-3):127-137.

Henriksson J and Reitman JS. 1977. Time course of changes in human skeletal muscle succinate dehydrogenase and cytochrome oxidase activities and maximal oxygen uptake with physical activity and inactivity. Acta Physiologica Scandinavica. 99(1):91-97.

Hill AV and Hartree W. 1920. The four phases of heat production in muscle. The Journal of Physiology. 54(1-2):84-128.

Hill AV, Long CNH, Lupton H. 1924. Muscular exercise, lactic acid, and the supply and utilization of oxygen. Proceedings of the Royal Society of London. Series B, Containing Papers of a Biological Character. 97(681):84-138.

Hoydal MA, Stolen TO, Johnsen AB, Alvez M, Catalucci D, Condorelli G, Koch LG, Britton SL, Smith GL, Wisloff U. 2014. Reduced aerobic capacity causes leaky ryanodine receptors that trigger arrhythmia in a rat strain artificially selected and bred for low aerobic running capacity. Acta Physiologica. 210:854-864.

Jiang ZY, Zhou QL, Coleman KA, Chouinard M, Boese Q, Czech MP. 2003. Insulin signaling through Akt/protein kinase B analyzed by small interfering RNA-mediated gene silencing. PNAS. 100(13):7569-7574.

Karp G. 2010. Cell and Molecular Biology. John Wiley and Sons. Hoboken, NJ. pp.631-633.

Koch LG, Britton SL. 2001. Artificial selection for intrinsic aerobic endurance running capacity in rats. American Physiological Society: Physiological Genomics. 5(1):45-52.

Koch LG, Britton SL. 2005. Divergent selection for aerobic capacity in rats as a model for complex disease. Integrative and Comparative Biology. 45(3):405-415.

Koch LG, Britton SL, Wisloff U. 2012. A rat model system to study complex disease risks, fitness, aging, and longevity. TCM. 22(2):29-34.

Koch LG, Kemi OJ, Qi N, Leng SX, Bijma P, Gilligan LJ, Wilkinson JE, Wisloff H, Hoydal MA, Rolim N, et al. 2011. Intrinsic aerobic capacity sets a divide for aging and longevity. Circulation Research. 109:1162-1172.

Krogh-Madsen R, Thyfault JP, Broholm C, Mortensen OH, Olsen RH, Mounier R, Plomgaard P, van Hall G, Booth FW, Pedersen BK. 2010. A 2-wk reduction of

ambulatory activity attenuates peripheral insulin sensitivity. Journal of Applied Physiology. 108(5):1034-1040.

Lammers G, Poelkens F, van Duijnhoven NTL, Pardoel EM, Hoenderop JG, Thijssen DHJ, Hopman MTE. 2012. Expression of genes involved in fatty acid transport and insulin signaling is altered by physical inactivity and exercise training in human skeletal muscle. Am J Physiol Endocrinol Metab. 303:E1245-E1251.

Lessard SJ, Rivas DA, Stephenson EJ, Yaspelkis III BB, Koch LG, Britton SL, Hawley JA. 2011. Exercise training reverses impaired skeletal muscle metabolism induced by artificial selection for low aerobic capacity. American Jounral of Physiology Regulatory, Integrative, and Comparative Physiology. 300(1):R175-R182.

Liu Y, Liu F, Grundke-Iqbal I, Iqbal K, Gong C. 2011. Deficient brain insulin signaling pathway in Alzheimer's disease and diabetes. Journal of Pathology. 225:54-62.

Lodish H, Berk A, Kaiser CA, Krieger M, Bretscher A, Ploegh H, Amon A. 2013. Molecular Cell Biology. Seventh Edition. W.H. Freeman and Company. New York, NY. pp.765-767.

Manning BD and Cantley LC. 2007. Akt/PKB signaling: navigating downstream. Cell. 129(7):1261-1274.

Medeiros C, Frederico MJ, Da Luz G, Pauli JR, Silva ASR, Pinho RA, Velloso LA, Ropelle ER, De Souza CT. 2010. Exercise training reduces insulin resistance and upregulates the mTOR/p70S6k pathway in cardiac muscle of diet-induced obesity rats. Journal of Cellular Physiology. 226:666-674.

Novak CM, Escande C, Burghardt PR, Zhang M, Barbosa MT, Chini EN, Britton SL, Koch LG, Akil H, Levine JA. 2010. Spontaneous activity, economy of activity, and resistance to diet-induced obesity in rats bred for high intrinsic aerobic capacity. Hormones and Behavior. 58(3):355-367.

Pollock ML, Foster C, Knapp D, Rod JL, Schmidt DH. 1987. Effect of age and training on aerobic capacity and body composition of master athletes. Journal of Applied Physiology. 62(2):725-731.

Rome S, Clement K, Rabasa-Lhoret R, Loizon E, Poitou C, Barsh GS, Riou JP, Laville M, Vidal H. 2003. Microarray profiling of human skeletal muscle reveals that insulin regulates ~800 genes during a hyperinsulinemic clamp. The Journal of Biological Chemistry. 278(20):18063-18068.

Rose AJ and Richter EA. 2005. Skeletal muscle glucose uptake during exercise: how is it regulated? Physiology. 20(4):260-270.

Samuel VT and Shulman GI. 2012. Mechanisms for insulin resistance: common threads and missing links. Cell. 148:852-871.

Sasson S, Edelson D, Cerasi E. 1987. In vitro autoregulation of glucose utilisation in rat soleus muscle. Diabetes. 36(9):1041-1046.

Short KR, Vittone JL, Bigelow ML, Proctor DN, Rizza RA, Coenen-Schimke JM, Nair KS. 2003. Impact of aerobic exercise training on age-related changes in insulin sensitivity and muscle oxidative capacity. Diabetes. 52(8):1888-1896.

Shulman GI. 2000. Cellular mechanisms of insulin resistance. The Journal of Clinical Investiation. 106(2):171-176.

Stanford KI and Goodyear LJ. 2014. Exercise and type 2 diabetes: molecular mechanisms regulating glucose uptake in muscle. Advances in Physiology Education. 38(4):308-314.

Tam CS, Xie W, Johnson WD, Cefalu WT, Redman LM, Ravussin E. 2012. Defining insulin resistance from hyperinsulinemic-euglycemic clamps. Diabetes Care. 35:1602-1610.

Taylor EB, An D, Kramer HF, Yu H, Fujii NL, Roeckl KSC, Bowles N, Hirshman MF, Xie J, Feener EP, Goodyear LJ. 2008. Discovery of TBC1D1 as an insulin-, AICAR-, and contraction-stimulated signaling nexus in mouse skeletal muscle. The Journal of Biological Chemistry. 283(15):9787-9796.

Timson BF, Falls HB, Wilson TE, Zimmerman SD. 2008. Effect of muscle strength on VO_2 plateau occurrence rate. Isokinetics and Exercise Science. 16:231-237.

Thyfault JP and Krogh-Madsen R. 2011. Metabolic disruptions induced by reduced ambulatory activity in free-living humans. Journal of Applied Physiology. 111(4):1218-1224.

Tremblay MS and Willms JD. 2003. Is the Canadian childhood obesity epidemic related to physical inactivity? International Journal of Obesity. 27:1100-1105.

Wasserman DH and Ayala JE. 2005. Interaction of physiological mechanisms in control of muscle glucose uptake. Clinical and Experimental Pharmacology and Physiology. 32:319-323.

White MF. 2003. Insulin signaling in health and disease. Science. 302:1710-1711.

Wisloff U, Najjar SM, Ellingsen O, Haram PM, Swoap S, Al-Share Q, Fernstrom M, Rezaer K, Jun Lee S, Koch L, Britton S. 2005. Cardiovascular risk factors emerge after artificial selection for low aerobic capacity. Science. 307(5708):418-420.

Wojtaszewski JFP, Hansen BF, Gade J, Kiens B, Markuns JF, Goodyear LJ, Richter EA. 2000. Insulin signaling and insulin sensitivity after exercise in human skeletal muscle. Diabetes. 49:325-331.

APPENDICES

Appendix A

Group assignments of LCR and HCR Rats

Group	Mass(g)*	Surgery Mass(g)	Clamp Mass(g)	ΔMass	Age (days)
HCR Catheterization	377.7	377	370.6	6.4	-
	404.3	410.2	370	40.2	-
	486.8	518.5	502.6	15.9	308
	399.2	420	408	12	286
	472.7	507	-	-	330
	472.6	499.9	474.5	25.4	298
	374.6	395.5	-	-	326
HCR Sham/Basal	403.2	400.6	392.9	7.7	247
	400.9	420.5	389.6	30.9	277
	471.6	482.2	480.8	1.4	305
	383.7	392.3	383.9	8.4	277
	481.5	510	479.4	30.6	339
	463.1	479.1	474	5.1	322
	384	411.2	408.5	2.7	354
LCR Catheterization	532.8	540	528	12	280
	509.3	526.6	408.2	118.4	296
	605.7	637.6	602.5	35.1	303
	507.6	523.4	507.5	15.9	302
	597.6	625.6	-	-	321
	485.8	509.4	463.5	45.9	338
	495.2	525.9	-	-	312
LCR Sham/Basal	531	531.1	-	-	303
	531.5	532.5	448.2	84.3	267
	559.7	596.8	-	-	300
	540.8	565	563.2	1.8	288
	472.3	488.1	-	-	338
	576.1	608	515.5	92.5	344
	525	553.1	545.1	8	335

This table displays group assignments for surgical groups. Rats were weight-matched to reduce variables. The * refers to mass measurement taken after 12-week observation, which determined group placement. Actual mass refers to measurement taken on surgery day while clamp mass refers to mass taken the morning of the euglycemic-hyperinsulinemic clamp. Clamp mass was the final mass taken before tissue harvesting. Change in mass was recorded to support adequate recovery from surgery and ages are displayed to support a negligible effect of age on surgical procedures and data collection.

Appendix B

Fecal samples were collected by Dr. Tyler Morris at the Jordan Valley Innovation Center. Total DNA was extracted using Qiagen QiAmp DNA Stool Mini Kit and was quantified using Nanodrop 2000 before subsequent dilution to 10 ng/µL. The protocol was modified slightly to yield a higher ratio of bacterial DNA to host DNA. About 50 ng DNA was loaded into a PCR reaction that targeted bacterial 16s rRNA variable regions V2 and V3 for species-specific identification. A 40 bp GC clamp was incorporated for purposes of separation in subsequent gel staining. After product verification, the samples were loaded into denaturing gradient gel electrophoresis (DGGE). The gel was then stained with Ethidium Bromide and imaged using UV transillumination.

From the gel image below, a similarity matrix was constructed using Phoretix software. Based on the similiarities, the UPGMA dendrogram below was constructed to show relationships between organismal microflora in LCR and HCR rats. These data suggest that aerobic capacity does not influence gut microflora. A similarity matrix was constructed with no less than 79% similarity between LCR and HCR samples. These data may further support the role of aerobic capacity within the cell, affecting mitochondrial dynamics or insulin signaling pathways. The observed difference in metabolism may therefore be attributed to aerobic capacity and cannot be associated with microflora composition.

A)

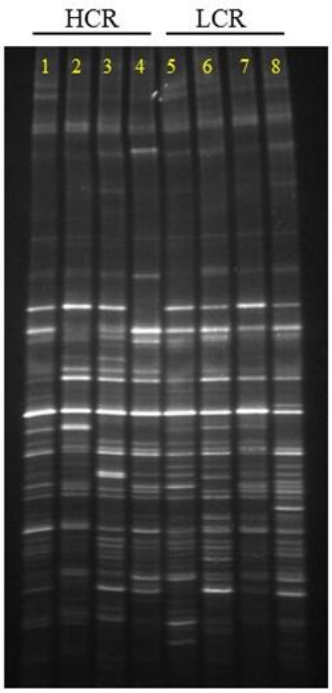

B)

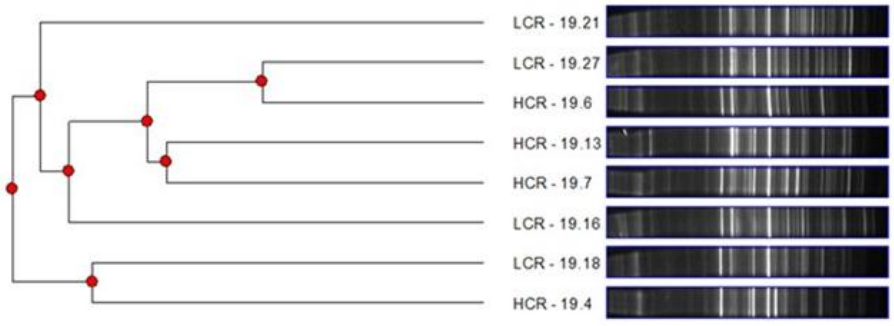

C)

Lane	19.6	19.14	19.7	19.13	19.16	19.27	19.18	19.21
19.6	100%							
19.14	90%	100%						
19.7	89%	84%	100%					
19.13	90%	88%	90%	100%				
19.16	88%	84%	82%	87%	100%			
19.27	93%	86%	90%	89%	90%	100%		
19.18	86%	88%	80%	84%	86%	88%	100%	
19.21	86%	79%	86%	85%	83%	88%	84%	100%

Gut microflora composition of LCR and HCR rats. Panel **A)** DGGE fingerprint generated from HCR and LCR samples. Lanes are as follows: (1) HCR - 19.6; (2) HCR - 19.14; (3) HCR – 19.7; (4) HCR – 19.13; (5) LCR – 19.16; (6) LCR – 19.27; (7) LCR – 19.18; (8) LCR – 19.21. Panel **B)** UPGMA dendrogram from fecal samples. This representation classifies and groups sample lanes on the basis of band presence/absence similarities. Panel **C)** Similarity matrix generated using Dice similarity index. The boxes shaded in green denote the comparisons within HCR samples, the Red boxes show comparisons within LCR samples, and the Blue boxes compare HCR samples to LCR samples.